AN ABSTRACT OF THE THESIS OF

Lynn Marie deWitt for the degree of Master of Science in the School of Oceanography presented on August 13, 1981

Title: Variability of the Upper Ocean Internal Wave Field During JASIN

Abstract approved: Redacted for privacy
Clayton A. Paulson

Temperature was measured at 21 depths in the upper 82 m of the ocean with three thermistor chains moored in the North Atlantic ($59^{\circ}00.2'$-$59^{\circ}10.7'$N, $12^{\circ}27.4'$-$12^{\circ}33.6'$W). The measurements were taken over a period of 40 days in August and September 1978 as part of the Joint Air-Sea Interaction Experiment (JASIN). Observations were analyzed to determine the character of the upper ocean internal wave field in that region. The isotherm displacement spectra calculated from these data were not consistent with the model of Garrett and Munk (1975). The slopes of the spectra were about half as steep as the slope of the model spectrum. Internal wave spectra which are not in agreement with the model spectrum may indicate the proximity of internal wave generation and dissipation mechanisms because the model describes an internal wave field far from strong sources and sinks, where the field has approached a universal state. Wind and topography were examined to determine the major source of internal wave energy during JASIN. The variation of the spectral levels in time was not significantly correlated with wind speed, which implies that the wind is not the dominant source of energy. Spectral peaks at semidiurnal frequency suggested that conversion of barotropic tidal energy into baroclinic motion was important in the region. A week-long

period of coherent, high-amplitude semidiurnal oscillations indicated that the signal was dominantly from one source during late August 1978. By use of the mooring array as a simple antenna, the two-dimensional wavenumber spectrum at tidal frequency was formed, and the semidiurnal internal tide was found to have a wavelength of about 36 km, making it dominantly third mode. The wavenumber spectrum and the nearby topography suggested that the internal tide propagated toward the northeast during late August and that the dominant source was Rockall Bank, about 100 km southwest of the mooring array.

Variability of the Upper Ocean Internal Wave Field During JASIN

by

Lynn Marie deWitt

A THESIS

submitted to

Oregon State University

in partial fulfillment of
the requirements for the
degree of

Master of Science

Completed August 13, 1981

Commencement June 1982

APPROVED:

Redacted for privacy

Professor of Oceanography
in charge of major

Redacted for privacy

Dean of the School of Oceanography

Redacted for privacy

Dean of Graduate School

Date thesis is presented August 13, 1981

Typed by Lynn Marie deWitt for Lynn Marie deWitt

ACKNOWLEDGEMENTS

I owe much to Dr. Clayton A. Paulson, my major professor, for his guidance and constructive comments, and to Dr. Murray D. Levine for his many helpful suggestions and for the physical insight into internal wave theory provided by our discussions.

My thanks go to Dr. Wayne V. Burt who proposed this experiment and has allowed me to use his data. I also gratefully acknowledge the cooperation of the officers, crew and scientists aboard the R/V ATLANTIS II, David F. Casiles, commanding and Melbourne G. Briscoe, Chief Scientist, and Jay Simpkins, James Wagner, and the personnel from the Woods Hole Buoy Group for their aid in deployment and retrieval of the moorings. The initial preparation of the data was done by Joseph Bottero. Especially helpful was software written by Thomas J. Spoering which formed the basis for the spectral and plotting programs used in this analysis.

Special thanks are extended to my husband, Webb, who provided moral support and patiently endured my long working hours.

This research was supported by the Office of Naval Research through contracts N00014-76-C-0067 and N00014-79-C-0004 under project NR 083-12.

TABLE OF CONTENTS

LIST OF FIGURES

VARIABILITY OF THE UPPER OCEAN INTERNAL WAVE FIELD DURING JASIN

1. Introduction

Although the deep ocean internal wave field has been studied extensively, there have been few studies of internal waves in the upper ocean. Gregg and Briscoe (1979) and Garrett and Munk (1979) have reviewed the theory and observations of internal waves. It has been found that deep ocean internal wave spectra have little variability and are usually in good agreement with the stationary model of Garrett and Munk (1972, 1975; hereafter referred to as GM). However, some upper ocean studies have found considerable variability of the internal wave field and deviation from the GM model (Roth, Briscoe and McComas, 1981).

The GM model describes the internal wave field far from strong sources and sinks where the field has approached its universal state. The model was not meant to apply in regions containing strong currents, steep continental slopes or rough bottom topography. It was also not intended as a description of internal waves in the upper ocean where the rapid variation of the Brunt-Vaisala frequency may violate requirements necessary to invoke the WKB approximation in solving the vertical structure of the internal waves.

Roth, Briscoe, and McComas (1981) have suggested that the variable upper ocean internal wave field can be represented as fluctuations superimposed on the stationary GM spectrum. However, the generation, dissipation, and interaction mechanisms which cause these fluctuations in the upper ocean internal wave field are not well

understood (Thorpe, 1975). As suggested by Wunsch (1976), internal wave fields which are not in agreement with the GM model provide valuable clues on the identification of sources and sinks of internal wave energy.

Wunsch (1976) and Wunsch and Webb (1979) searched many internal wave records for departures from the GM spectrum. They found most measurements to be in close agreement with the energy levels predicted by GM, but found that topographic features such as seamounts and canyons cause deviations in the spectrum which suggests that these features are likely to be internal wave sources. They further showed that the influence of the topography is rapidly reduced away from the source (about 1 km vertically and 10 km horizontally) implying that dissipation is also strong in these regions.

The data used in the present study were obtained from an array of thermistor chains moored in the North Atlantic during July, August, and September of 1978 as part of the Joint Air-Sea Interaction Experiment (JASIN). Temperature was recorded at ten-minute intervals at 21 depths in the top 82 m of the ocean. These observations, described in Section 2, were taken in the upper ocean, in a region with an abundance of nearby topographic features (Fig. 1) so one might not expect to find good agreement with the GM model. The average moored isotherm displacement spectra is described in Section 3 and compared with the GM spectrum. In section 4, the temporal variation of the spectra is discussed for two frequency bands, and the correlation between the internal waves and the strength of possible generators such as the wind is examined.

Internal wave observations contain large amounts of energy at semidiurnal tidal frequency. Wunsch (1975a) and Hendershott (1981) review the theory and observations of

internal tides. A concise review of the generation of internal tides by interaction of the barotropic tide with a continental shelf and slope is found in Torgrimson and Hickey (1979). Estimation of the frequency-wavenumber spectrum is one method of analyzing array data to determine the wavelength and directional properties of signals. This method was used in the study of the propagation of surface gravity waves (Regier and Davis, 1977) and of the internal tide (Wunsch and Hendry, 1972). Hendry (1977) determined the direction of the open-ocean internal tide in the western central Atlantic during the Mid-Ocean Dynamics Experiment (MODE). He was able to identify the Blake Escarpment, 700 km from the experimental area, as the most probable generation region, and found the internal tide to be dominantly first mode. In Section 5, a week-long period of high-amplitude semidiurnal internal tides is analyzed to determine the direction of propagation of the waves, their wavelength, and the probable location of the region in which the waves were generated.

2. Observations

JASIN was a joint experiment with participants from ten countries. It took place in the North Atlantic in an area centered on Rockall Channel (57° to 60° N, 10° to 15° W) about 200 to 400 km off the west coast of Scotland. Meteorological and oceanographic data were gathered during July, August, and September of 1978 using buoys, ships, balloons, and aircraft. The operational and scientific plans for JASIN are described in detail by the Royal Society (1977, 1978) and have been summarized by Pollard (1978).

The observations used in the present study were obtained at JASIN moorings B1 through B4. The location of these moorings is shown in Fig. 1, along with the location of other moorings in the JASIN project. Moorings B1, B2, and B3 were located in an area called the Fixed Intensive Array (FIA), with mooring B4 about 20 km to the north. Each mooring included two Aanderaa recorders and thermistor chains which sampled water temperature at ten minute intervals. At moorings B2, B3, and B4, eleven thermistors on shallow chains measured temperature at vertical separations of 3 m from a depth of 5.5 m to 35.5 m. A loop in the cable at mooring B1 caused the shallow chain at this mooring to be one meter more shallow than at the other three, so observations there were at vertical separations of three meters from 4.5 m to 34.5 m. The deep thermistor chain at all four moorings measured temperature at ten locations separated by intervals of five meters from a depth of 36.5 m to 81.5 m. The eleventh channel on the deeper chains was used to record pressure, but because of an apparent sensor malfunction, pressure observations have not been included in this analysis. Measurements from buoy B3 were

Fig. 1. Location of the four moorings B1, B2, B3, and B4 in relation to the topography and other moorings in the JASIN project. Section lines correspond to profiles of topography in Fig. 11.

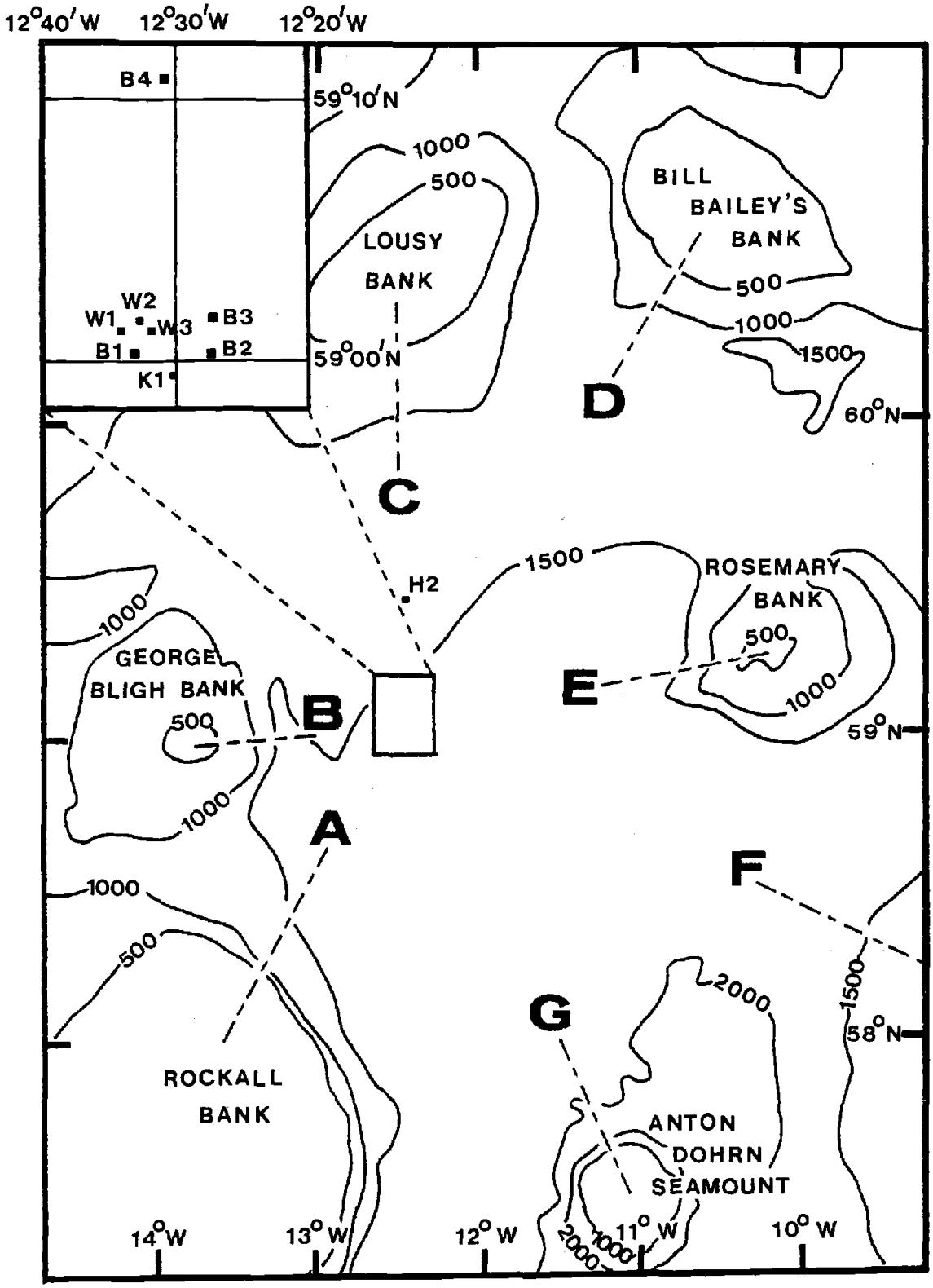
12°40′W
12°30′W
12°20′W
B4
59°10′N
1000
500
LOUSY
BANK
BILL
BAILEY'S
BANK
500
1000
1500
60°N
W2
W1
W3
B3
B1
B2
59°00′N
K1
D
C
H2
1500
ROSEMARY
BANK
500
1000
59°N
1000
GEORGE
BLIGH BANK
500
B
E
1000
A
F
1000
500
2000
1500
58°N
G
ROCKALL
BANK
ANTON
DOHRN
SEAMOUNT
14°W
13°W
12°W
2000
1000
11°W
10°W

Fig. 1

extremely noisy and have also been excluded. Most of the sensors on the deep chains at the other moorings were in operation for the entire experiment, but most of the shallow thermistors failed by the middle of August. Complete sets of temperature observations for each of the moorings B1, B2, and B4 as well as details of the duration of the temperature sensors are presented by deWitt, et al (1980).

Depths of isotherms 0.2° C apart were computed as a function of time for each mooring by linear interpolation between adjacent temperature measurements. Except when inversions occur, the vertical direction in which the interpolation proceeds is not important. The problem of inversions was handled by taking the average of the two sets of values of isotherm depth obtained by interpolation down from the most shallow sensor and interpolation up from the deepest sensor. A time series of the difference between isotherm depths computed in the two directions showed that inversions occurred infrequently enough to justify this procedure for the purpose of this analysis. Less than 0.5 percent of the total isotherm depths were computed by averaging two differing values. Most of these values differed by less than 5 m, only four percent were over 15 m, and no differences were larger than 30 m. Most inversions occurred at mooring B1, where 1.3 percent of the isotherm depths were averaged as the result of an inversion. Of these, 84 percent occurred at a depth of about 35 m where the upper and lower thermistor chains were within 2 m of each other. These particular inversions can probably be attributed to uncertainty in calibration, but most of the other inversions encountered were probably real. The maximum number of isotherm depths where inversions were encountered on any one day,

including mooring B1, was less than five percent of the isotherm depths from that day.

Isotherms which were at least 80 percent complete on a given day were completed by linear extrapolation from adjacent isotherms. Isotherms which strayed from the depth range of the temperature sensors did not meet this criterion and were excluded from the analysis. Twelve hour averages of isotherm depth for each mooring are shown in Fig. 2. Only that portion of the data which is used for spectral analysis in the next section is presented.

Sea surface temperature and atmospheric conditions were also recorded at each of the moorings B1 through B4 and have been analyzed by Ishida (1980). According to Ishida, a high pressure system in the Norwegian Sea during early August resulted in winds from the North at the FIA. Wind speed measurements (Fig. 2) from all moorings were similar, therefore only those from mooring B1 are presented. The winds reached a maximum of 15 m/s on August 20 and the sea surface temperature decreased by about 1° C. The resulting increase in the depth of the seasonal thermocline can be seen as a rapid deepening of the upper isotherms at this time in Fig. 2. The deepening is more apparent at mooring B2 than at the other two moorings because more of the shallow sensors were operational at mooring B2 at this time. On about August 23, the winds decreased and the sea surface temperature increased by about 1° C over a period of several days. During late August a stationary high west of England caused winds from the west at the FIA.

Other features observed in the average isotherm depths cannot be related directly to atmospheric forcing and may be the result of advection of frontal structures

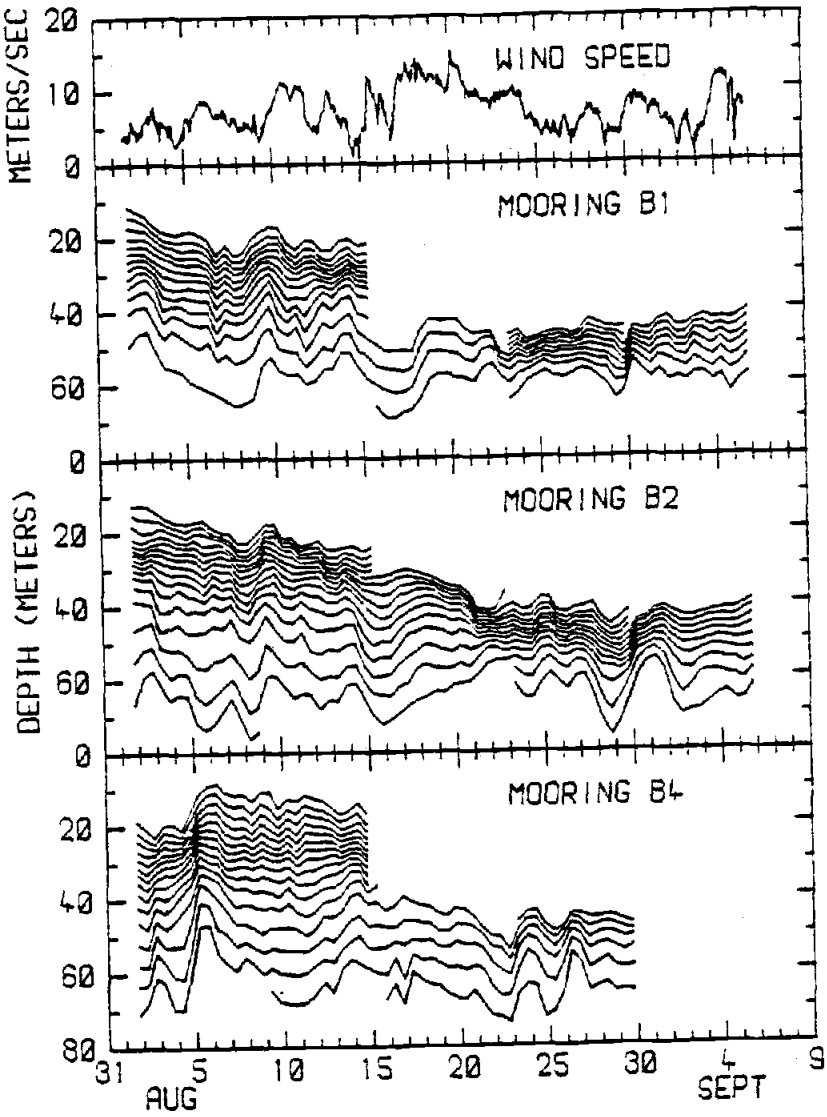

Fig. 2. One hour averages of wind speed at the mooring array and twelve hour averages of isotherm depth for isotherms used in spectral analysis. Isotherms are 0.2° C apart and the top isotherms shown on August 1 are 12.8° C for moorings B1 and B2, and 12.6° C for mooring B4.

past the moorings. For example, a large low frequency oscillation appeared in twelve hour averages of isotherm depth on August 28 to 30 at mooring B2 and to a lesser extent at mooring B1 (Fig. 2). This oscillation appears to be the feature discussed by Joyce, Käse, and Zenk (1980) in their study of data from moorings K2 and K3 (Fig. 1). By use of current meter data and a simple model, Joyce, Käse, and Zenk showed that this feature was probably the result of advection of a front past the moorings. An even larger frontal structure appeared to move past mooring B4 on August 4 to 5 (Fig. 2). The depth of the deeper isotherms decreased by almost 25 m over a period of a few days. In this case the isotherms did not return to their original depth, but remained about 15 m more shallow than they were prior to the frontal passage.

According to Tarbell, Briscoe, and Weller (1979), the mean current at mooring W2 (Fig. 1) abruptly changed direction from northwest to southwest around August 20. At mooring H2, 50 km north of the FIA, the current reversal took place around August 5 (Halpern, personal communication).

Pollard (1981) offers the most probable explanation for the observed frontal structure and shift in mean current. Pollard's analysis of salinity data from CTD surveys during JASIN suggests that large areas of anticyclonic circulation positioned on either side of the FIA moved westward during August 1978. Van Aken and Prangsma (1981) describe what appear to be the same feature discussed by Pollard. They estimate the propagation speed of these meanders or eddies to be about 2 km per day, and the typical cross horizontal length scale of the fronts associated with them to be about 2 to 6 km. This is consistent with a front passing a mooring in two to three days.

3. Average Spectra

As previously discussed, deviation of internal wave spectra from the GM spectrum may suggest the proximity of sources or sinks of internal wave energy. In this section the average isotherm displacement spectra from moorings B1, B2, and B4 are described and compared with the GM spectrum. The temporal variation of the spectra is discussed in the next section.

The time series of isotherm depths calculated as described in the previous section were each divided into segments of 1024 points (170.67 hours) for spectral analysis (Table 1). At the expense of excluding some data from mooring B4, the segments were selected to cover the same time periods at each mooring.

Spectra of isotherm depth were computed for all isotherms which were complete during a given segment by use of a Fast Fourier Transform (FFT) algorithm. As suggested by Frankignoul (1974), each demeaned series was prewhitened by taking the first forward difference before the FFT was applied. The series was then recolored by dividing by the transform of the differencing scheme. Frankignoul found this method to be more appropriate than data windowing to reduce contamination produced by end point jump in analysis of internal wave records of short length. He showed that both methods reduce the jump effect, but that data windowing of records with large inertial or tidal peaks results in more leakage of energy from the peaks into adjacent bands.

Ensemble averages of spectra from each mooring are shown in Fig. 3. These spectra have been smoothed at frequencies above 0.115 cph by band averaging into 15 nonoverlapping frequency bands per decade, equally spaced

Table 1. Time periods used for spectral analysis.

Segment	Start	End
1	1 Aug 1220	8 Aug 1450
2	8 Aug 1500	15 Aug 1730
3	15 Aug 1740	22 Aug 2010
4	22 Aug 2020	29 Aug 2250
5	29 Aug 2300	6 Sep 0130

on a logarithmic scale. No band averaging was performed below 0.115 cph. The spectral level at mooring B4 was higher on average than the level at B1 or B2, but levels were similar at the frequency of the semidiurnal tide (8.05×10^{-2} cph). The tidal peak is the most prominent feature in the spectra and is larger than the inertial peak ($7.144 - 7.156 \times 10^{-2}$ cph) by a factor of four or more at all three moorings. At frequencies just below the inertial frequency the spectral levels decrease sharply, but rise again at lower frequencies. At frequencies higher than the tidal peak, the spectra decrease with a slope of about ω^{-1}, and a small peak is evident at twice semidiurnal frequency. There is a suggestion of some flattening in spectral slope forming a shoulder at about 1 cph. This feature is more prominent in spectra from individual segments, where a peak at 1 cph is even evident in some cases. Above this shoulder, one might expect a sharp cutoff at the buoyancy frequency. The mean depth of the isotherms which were ensemble averaged in Fig. 3 is 50 m. The mean buoyancy frequency profile during JASIN (Fig. 4) has a maximum near this depth and varies rapidly over the depth range of the temperature sensors from 2 to 8 cph. Since the Nyquist frequency is 3 cph, a sharp cutoff at the buoyancy frequency might not be resolvable.

The spatial structure of the internal wave field can be characterized by the coherence between time series of isotherm depth separated vertically and horizontally. Before computing vertical coherence, cross-spectra of isotherm displacement pairs from each segment were grouped and averaged according to mean vertical separation regardless of actual mean depth. To reduce the possibility of introducing artificially high coherence, pairs of isotherms which were calculated from the same pair of

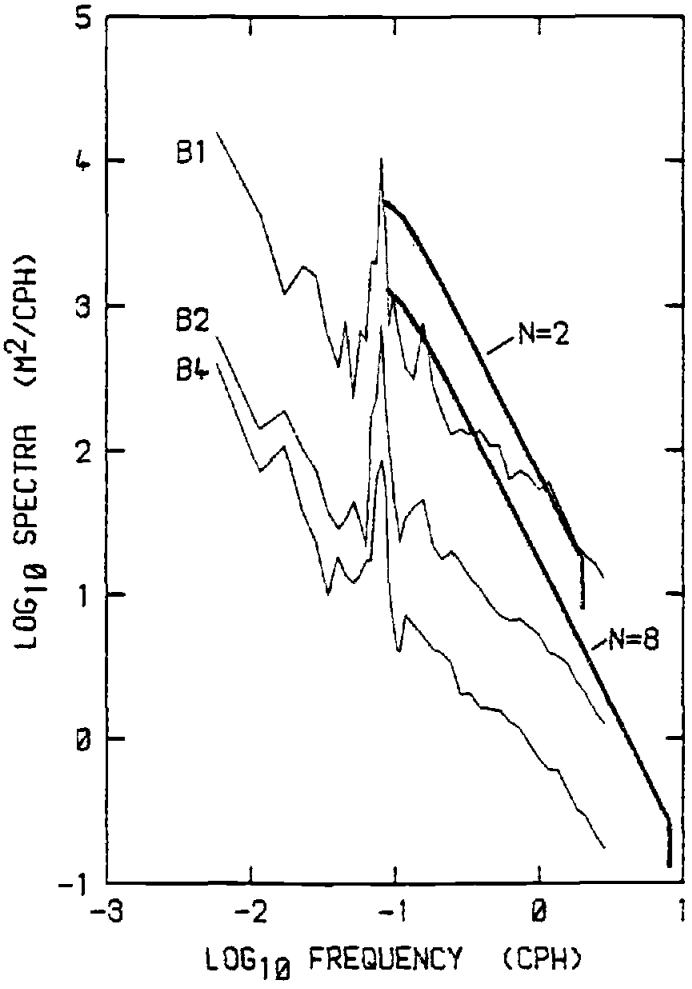

Fig. 3. Ensemble averages of isotherm displacement spectra for three isotherms from each mooring which were complete during all five segments used for spectral analysis. The vertical scale is for the spectrum from mooring B2. Spectra from moorings B1 and B4 are offset by one decade upward and one decade downward respectively. The mean depth of the isotherms which have been used is 50 m. Also plotted on the spectrum from B1 is the Desaubies' representation of the GM model (1) for r = 300 m^2cph and two values of buoyancy frequency.

sensors more than 20 percent of the time were excluded.

Vertical coherence was high for all vertical separations at nearly all frequencies during the entire observational period as shown by an ensemble average of the coherence for three separations from all five segments from mooring B2 (Fig. 5). Similar coherences were found at the other two moorings, but B2 is shown because there are more data at the largest separation. A sharp peak in vertical coherence occurs at all separations at tidal frequency, and a broader peak occurs at about 1 cph. There is also a suggestion of a peak for separations up to 15 m at about 0.16 cph, twice the frequency of the semidiurnal tide. Coherence was high at tidal frequency during all segments but increased for all separations during segment 4 (Fig. 7d).

Horizontal coherence between moorings was generally low (below the 95 percent significance level) with one exception. During segment 4, the coherence at a separation of 5.8 km between moorings B1 and B2 at tidal and inertial frequencies increased to very high levels (0.95 to 0.99) at all depths (Fig. 7c). Although the coherence for the two larger separations (B1-B4 and B2-B4) was higher at tidal frequency than at adjacent frequencies during segment 4, it was below the 90 percent siginificance level.

To relate the internal wave field at JASIN to other internal wave observations, the computed spectra were compared with the GM model using the analytical representation of the GM moored internal wave spectra $MS(\omega)$ proposed by Desaubies (1976):

$$MS(\omega) = \frac{2}{\pi} r \frac{f}{N(z)} \frac{(\omega^2 - f^2)^{\frac{1}{2}}}{\omega^3}, \qquad (1)$$

where f is the Coriolis parameter and N(z) the Brunt-Vaisala frequency. The parameter r has units of m^2cph

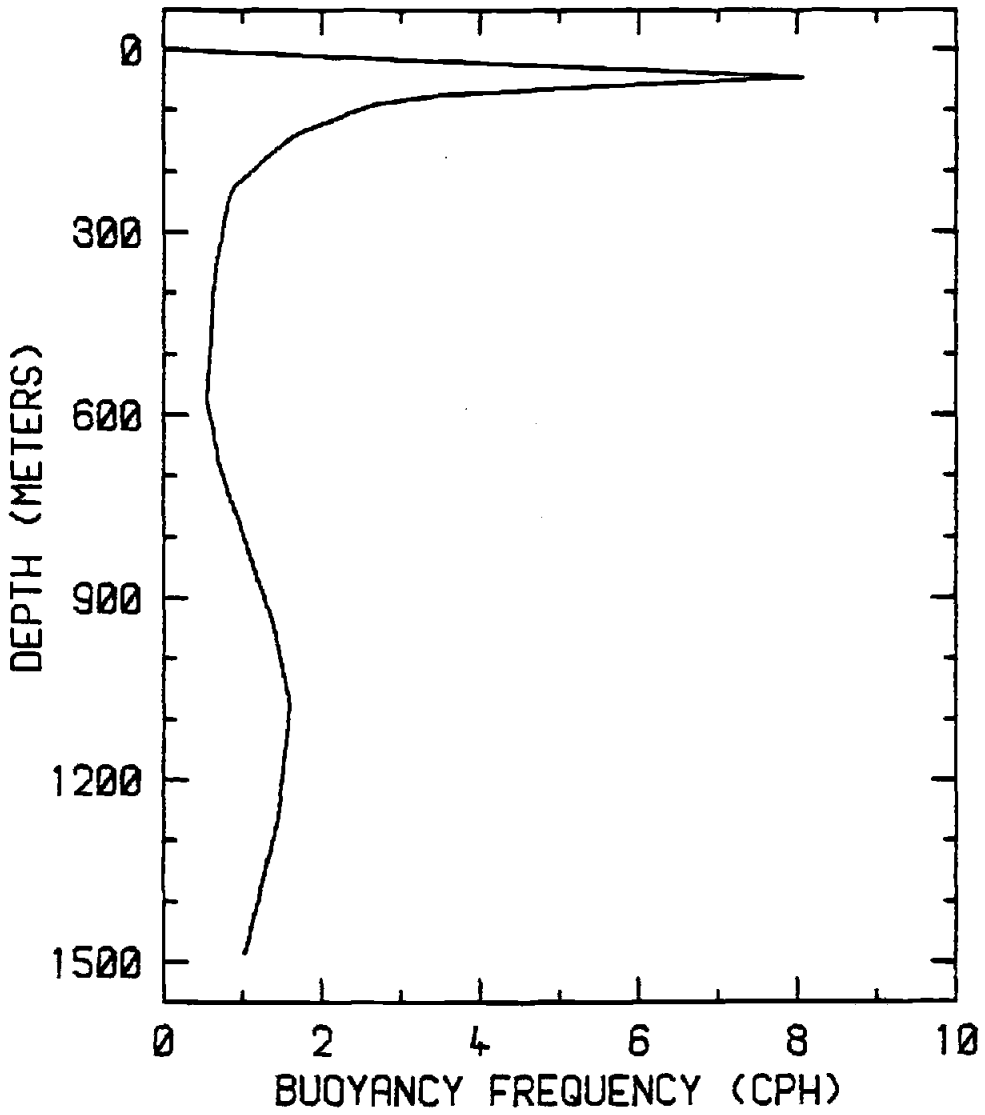

Fig. 4. Mean buoyancy frequency profile during JASIN. The profile is a smooth representation of a profile calculated by Tarbell, Briscoe, and Weller (1979) from CTD casts during the experiment.

and is related to the three parameters in the GM formulation by $r = Eb^2n$, where b and n control the shape and amplitude of an assumed exponential buoyancy frequency profile $N(z) = n\exp(-z/b)$, and E is a non-dimensional parameter which characterizes the energy level of the process. By integrating the equation for $MS(\omega)$ it can be shown that the parameter r is also related to the total vertical displacement variance (σ^2) by $\sigma^2 \cong r/2N$. Desaubies' parameterization is a simplification of the GM representation because it eliminates the need for assumptions about the specific shape of the buoyancy profile. The only other environmental parameter remaining in the model is then the ratio of the Brunt-Vaisala frequency to inertial frequency (N(z)/f). Desaubies found the value of r from deep ocean measurements is about 300 m^2cph with a maximum variation of a factor of two.

$MS(\omega)$ is compared with the observed spectra in Fig. 3 for an r of 300 m^2cph. It is clear that the slopes of the measured spectra (approximately ω^{-1}) are much less than predicted by the GM model (ω^{-2}). These results are unlike most deep ocean observations which generally agree with the GM model. For example, results of the Internal Wave Experiment (IWEX) at depths from 600 m to 2000 m in the Sargasso Sea showed that the internal wave field was horizontally isotropic and vertically symmetric except at tidal and inertial frequencies, and showed the spectra were in good agreement with the GM spectrum (Muller, Olbers, and Willebrand, 1978). Roth, Briscoe, and McComas (1981) compare five sets of upper ocean internal wave data with the best fit of the GM model to the deep ocean IWEX spectrum. Some of the upper ocean observations are in reasonable agreement with the model. For example,

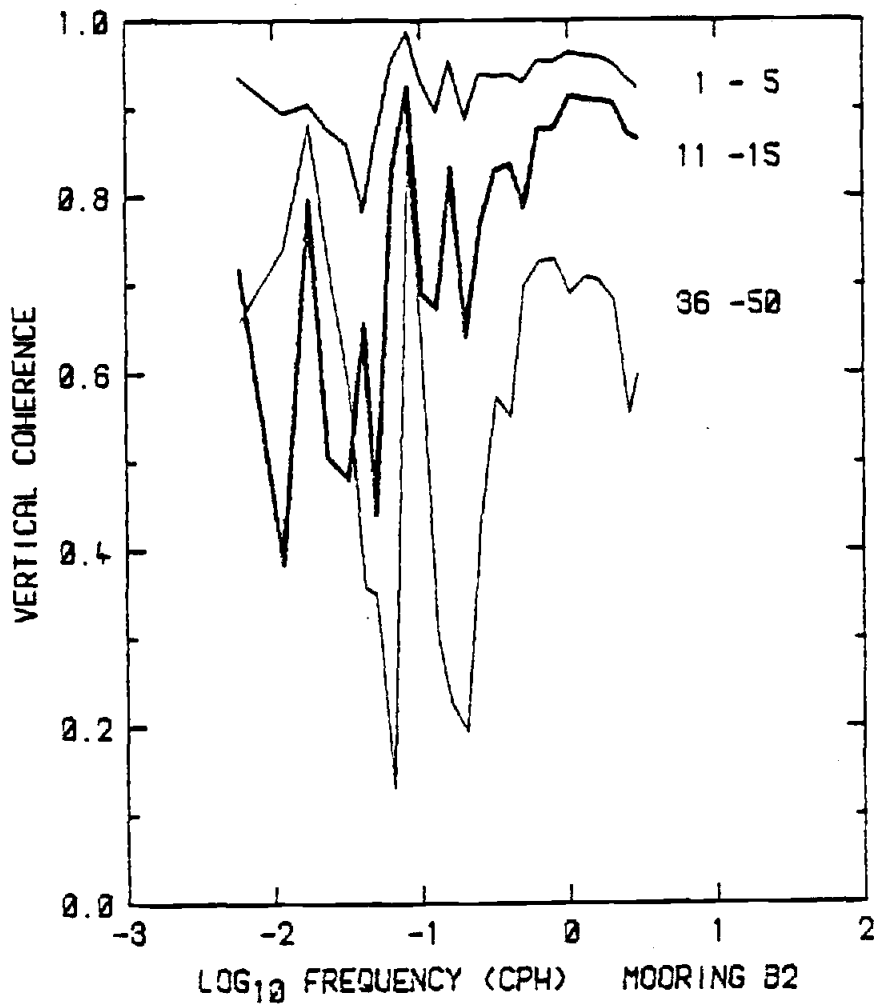

Fig. 5. Ensemble averages over all five time segments of coherence between isotherms from mooring B2 which have vertical separations of 1-5 m, 11-15 m, and 36-50 m, regardless of actual mean depth.

internal wave observations from FLIP in the upper 440 m of the Pacific Ocean (Pinkel, 1975) were in reasonable agreement with the GM spectrum at frequencies below 2 cph. Other upper ocean spectra indicate strong deviations from the model. For example Kase and Siedler (1979) found the slope of the average internal wave spectrum during the GARP Atlantic Tropical Experiment (GATE) was about $\omega^{-1.5}$ in most of the internal wave range and was even less steep above 1 cph. Levine and deSzeoke (1981) analyzed observations from a string of current meters at depths from 41 m to 175 m in the North-East Pacific during the Mixed Layer Experiment (MILE). Although they found that a spectral slope of $\omega^{-1.6}$ was a better fit than the ω^{-2} of the GM spectrum, their displacement spectra agree fairly well with the model except at tidal frequency and at frequencies above 1 cph.

Comparison of the spectra from the present study and the GM spectrum shows that not only are the slopes markedly different, the coherences and the total integrated energy of the two are also in poor agreement. The GM model predicts moored vertical and horizontal coherences that are fairly constant or slowly decreasing with frequency at a given separation out to frequencies close to the buoyancy frequency. The valleys and peaks in the coherences measured here, especially the broad peak in vertical coherence at about 1 cph (Fig. 5), are not consistent with the model. The mean buoyancy frequency varies from 2 to 8 cph over the depth range of the temperature sensors. The proper choice of N in the Desaubies representation of the GM model is uncertain but, as evident in Fig. 3, a larger value than 8 cph would be needed to make the total integrated energy levels similar. The value of r could also be adjusted, but the point to be

made here is that these observations are not consistent with the GM model. As noted by Wunsch (1975b), "it is the deviations from the Garrett-Munk models that experimentors should be looking for, that 'fiddling' the parameters of the models to fit any particular set of observations is ultimately self-defeating."

5. Temporal Variability of the Spectra

According to Wunsch (1976), lack of agreement with the GM spectrum suggests the presence of sources or sinks of internal wave energy. One way of examining sources of internal wave energy is to study the variation of spectral levels in time to determine the correlation with other oceanic and atmospheric events. In this section, the variation of spectral levels in two different frequency bands is discussed. The temporal variability in a high frequency band (0.5-2.0 cph) is examined and compared to the wind. The variation in spectral levels at semidiurnal frequency is also studied, and conversion of semidiurnal barotropic tidal energy into baroclinic motion on continental slopes is discussed in the next section.

Wind forcing is one proposed source of internal wave energy. To determine the effect of the wind on the internal wave field during JASIN, the segments used above were subdivided into segments of 128 points (21.33 hours) and spectral analysis was performed in the manner previously described. Fig. 6 shows the average spectral level in the band 0.5 cph to 2.0 cph for each 128 point segment as a function of time for each mooring. This band was chosen because it spans the broad peak in the vertical coherence at high frequency (Fig. 5) and represents a weak plateau or shoulder in the displacement spectra (Fig. 3). Comparison of the temporal variation in the energy level of this high frequency band with a time series of the wind (Fig. 6) shows very little correlation between the two. For example, the variance increases at all three moorings toward the end of August when the winds have dropped to a low level. The correlation coefficient between the spectral level in the high

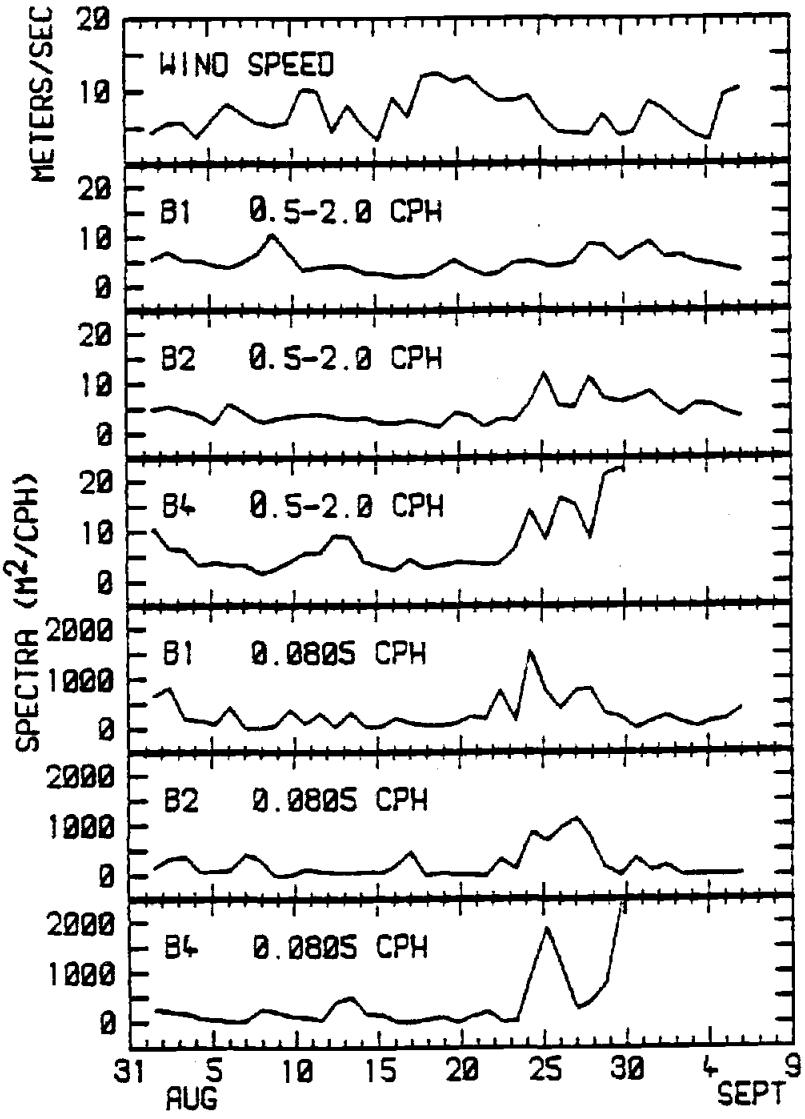

Fig. 6. Time series of averages over 21.33 hour intervals of wind speed, spectral levels in the high frequency band (0.5-2.0 cph), and spectral levels at M2 tidal frequency (0.08051 cph) at 50 m depth at moorings B1, B2, and B4. The isotherms used are indicated in the Appendix.

frequency band and the wind speed was -0.3 to -0.4 for all three moorings, which is not significantly different from zero at the 95 percent level.

As shown by the large tidal peaks in the ensemble averaged spectra from moorings B1, B2, and B4 (Fig. 3), the upper ocean during JASIN contained significant amounts of energy at semidiurnal tidal frequency. Although the tidal signal was large during the entire experiment, three hour averages of isotherm depth showed that it increased dramatically for about a week during late August. At all three moorings, the amplitude of semidiurnal oscillations from August 23 to 30 was more than twice as large as it was during any other time period. The manifestation of this event in spectral levels and coherences measured during the experiment is shown in Fig. 7, where segment 4 corresponds to the time period during which the amplitude of oscillation was high (Table 1). The changes in the variance with time in the tidal band (Fig. 7a) was similar at moorings B1 and B2. The variance greatly increased during segment 4, and then fell during segment 5 to a level slightly below that of any previous segment. The large changes in variance during segment 4 and 5 at these two moorings were accompanied by corresponding changes in horizontal coherence (Fig. 7b). Very high coherence was observed between moorings B1 and B2 during segment 4 at all depths, and coherence decreased rapidly as the variance fell during segment 5. The increase in variance at mooring B4 was even larger than at the other two moorings, but coherence at the larger horizontal separations (B1-B4 and B2-B4) fell slightly during segment 4 instead of increasing as it did between B1 and B2. The increase in variance in the tidal band during segment 4 was also accompanied by extremely high vertical coherence for all vertical separations at all three moorings. Fig. 7c illustrates this

Fig. 7. Variation of the variance at tidal frequency of isotherms at about 50 m depth (a), the horizontal coherence between isotherms at each mooring (b), and vertical coherence at mooring B2 for isotherms which have various vertical separations, regardless of actual mean depth (c). Points correspond to time periods in Table 1, and isotherms used in (a) and (b) are indicated in the Appendix.

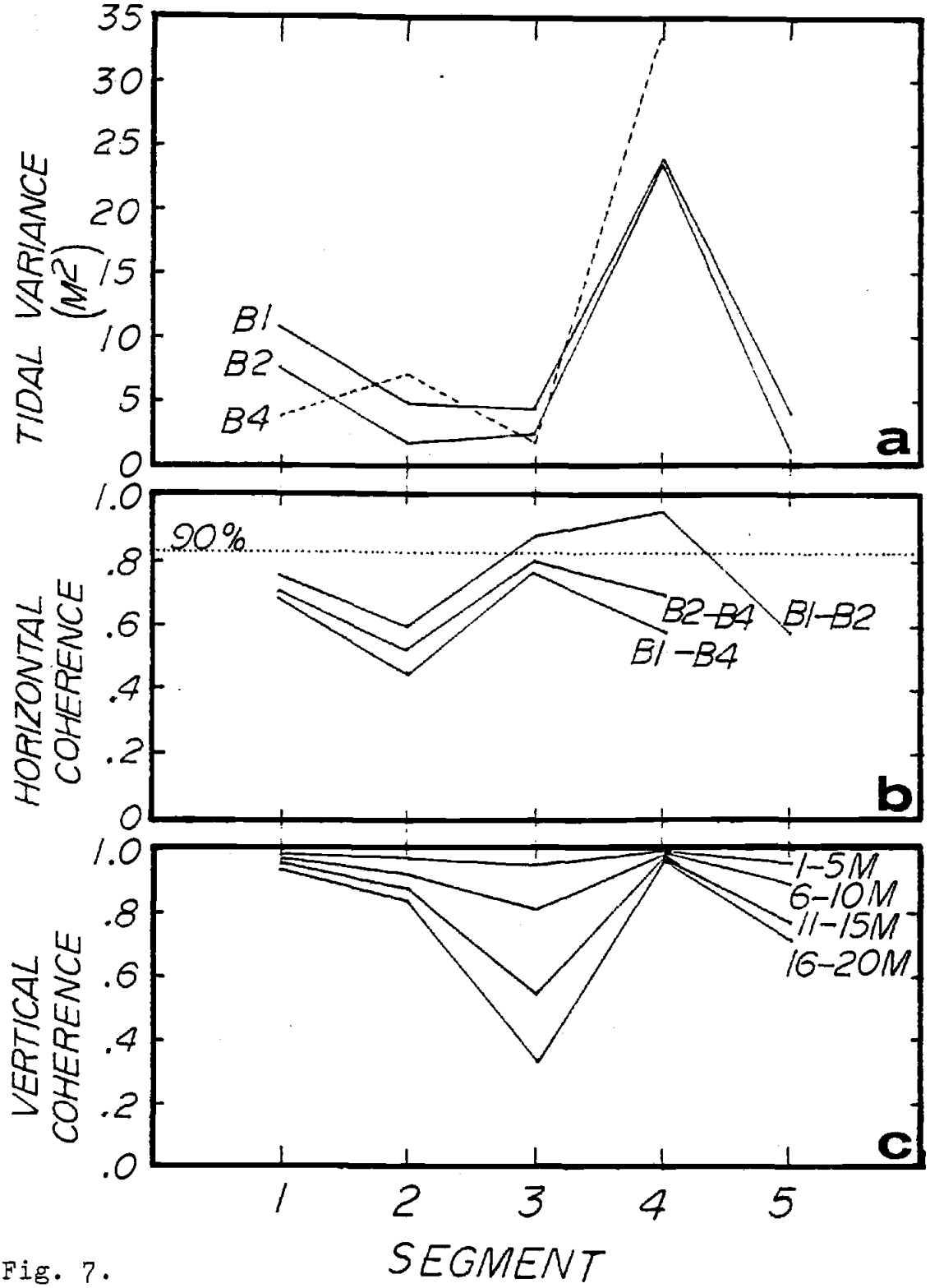
TIDAL VARIANCE (M²)
35
30
25
20
15
10
5
0
B1
B2
B4
a
HORIZONTAL COHERENCE
1.0
.8
.6
.4
.2
0
90%
B2-B4
B1-B2
B1-B4
b
VERTICAL COHERENCE
1.0
.8
.6
.4
.2
.0
1-5M
6-10M
11-15M
16-20M
c
1
2
3
4
5
SEGMENT

Fig. 7.

for mooring B2 where more data was available at the largest separations. It should be noted that the large decrease in coherence shown during segment 3 in this figure is not necessarily representative of moorings B1 and B4, but that the high coherences during segment 4 occurred to the same extent at all three moorings.

To study the sudden increase in amplitude of the semidiurnal internal tide during late August, and to examine the effect of energy input at tidal frequency on other internal wave scales, it is useful to investigate the correlation of the tide with smaller- and larger-scale events. The changes which characterize the high amplitude tidal oscillations and the events which occur simultaneously in the mean hydrographic field have been discussed above and in previous sections and are summarized as follows:

1) A large increase in the spectral levels at tidal frequency (Fig. 7a) occurred during late August which was accompanied by a large increase in vertical coherence for all vertical separations at all moorings (Fig. 7c), and a large increase in horizontal coherence between moorings B1 and B2 (Fig. 7b).
2) The spectral levels at high frequencies (0.5-2.0 cph) were also larger during late August, and these increases cannot be attributed to energy input from the wind (Fig. 6).
3) The large amplitude tidal oscillations occurred during a period of relatively low winds and began just as the wind decreased from a period during which it attained its maximum value during the experiment.
4) The mean current at the FIA changed direction abruptly from northwest to southwest within a

period of a few days from August 20 to 22 just before the large amplitude oscillation began (Tarbell, Briscoe, and Weller, 1979).

To quantitatively determine the correlation between the first three of these events, the variation of the internal tide was studied over smaller segments than the 1024 point segments used in Fig. 7. Spectral analysis was performed over 128 point segments at the frequency of the M2 semidiurnal internal tide (0.08051 cph). As discussed by Wunsch (1975a), the relatively short wavelength of the internal tides makes them susceptible to Doppler-shifting by more energetic currents. This shifting will tend to smear the energy in a band surrounding the appropriate tidal frequency. Changes in the mean currents and density structure in the region can have the same effect. Therefore, estimates of amplitude and energy should include the energy found in the sidebands as well as the energy at precisely the tidal frequency. To determine the contribution of these sidebands, spectral analysis was also performed over 128 point segments 0.005 cph on either side of M2 tidal frequency. The spectral levels at each of the three frequencies were similar during most segments, indicating that while the tidal peak was smeared into adjacent frequencies, the variation of the levels at tidal frequency are representative of the variation of the entire tidal band. The variation of the spectral level at M2 tidal frequency with time at the three moorings is shown in Fig. 6. Correlation between these series and the energy in the high frequency band gave correlation coefficients of 0.09, 0.46, and 0.73 for moorings B1, B2, and B4 respectively. It is unclear why the correlation is so much higher at mooring B4. As was found for the high frequency band, there was little correlation between the variation of the spectral level at tidal frequency and

wind speed. Correlation coefficients were about -0.3 between the wind and tidal variance at B2 and B4 and about -0.006 for B1. Therefore, while significant correlation may exist between the tidal and high frequency bands, wind forcing does not appear to be a source of energy for either of these bands.

As was discussed in Section 2, the currents during the observational period formed a complicated pattern of eddies which could contain regions of strong mean velocity shear. Ruddick and Joyce (1979) review studies on the interaction of an internal wave field with a mean shear flow and investigate the magnitude of this interaction in observations from four moorings in the North Atlantic during POLYMODE. They conclude that, on average, the mean flow is a source for internal wave energy, but a relatively minor one. From the present data alone it is not possible to quantitatively examine the effect of the mean flow on the internal wave field at JASIN, but its role in modifying the propagation characteristics of the internal tide can be qualitatively considered. As discussed previously, the sudden change in the direction of the current at the FIA during late August was probably the local result of a much larger scale meander or eddy which propagated towards the west during August 1978 (Pollard, 1981). The sudden increase in amplitude of the internal tide just after the current changed direction may be an indication that this event was due to a change in the character of the ocean between the mooring array and the generator, rather than to a change in the tidal source. Topographic generation of the internal tide is discussed in the next section. At this point it is sufficient to note the abundance of seamounts and banks in the JASIN region (Fig. 1) which may be able to convert barotropic tidal energy into baroclinic motion. A study of the barotropic tides near the FIA

during the experiment (M. D. Levine, personal communication) showed no evidence of extremely high tides which could cause a large change in the tidal signal during late August. However, even if the sources of the tidal signal were relatively constant during the observational period, a change in the mean current field could have changed the source of the signal received at the FIA. As discussed by Wunsch (1975a), energetic beams of internal tides can be moved comparatively large distances by current shifts.

Changes in the mean current between the generator and the mooring array can also affect horizontal and vertical coherences which are observed in internal tide studies. According to the theory of Rattray, Dworski, and Kovala (1969), the internal tide generated at a step-like shelf propagates along beam-like characteristics which are a coherent sum of many modes. Since the relative phase between these modes is fixed, a coherence of unity is expected between observations at stations very near an internal tide generator. However, as discussed by Munk and Phillips (1968), tides are usually found to be incoherent with respect to one another and with respect to tide producing forces. Munk and Phillips show that such incoherence, both vertically and horizontally, can result when modes at the same frequency bear no fixed phase relation to one another. These random phase relations can occur if modes are generated by independent random processes, or if they are coherently generated and then randomized by propagation through oceanic density fluctuations and fluctuations of mean flows which are comparable to internal wave phase speeds. It is for this reason that incoherent low modes rather than beamlike features are observed in deep ocean internal tide studies.

The mean circulation in the JASIN region, then, could have had at least two effects on the character of the tidal

signal received at the FIA besides the smearing of the peak due to Doppler-shifting. First, fluctuations in the mean flow act ot reduce vertical and horizontal coherence between tides generated by different topographic features, and between modes generated by a single source. Second, the observed propagation of large meanders through the experimental area may have changed the dominant source of the signal received at the mooring array. These two effects probably acted together to produce the large variation in the internal tide discussed above. For example, some topographic features in the region are better generators than others, and the strongest signals are probably received from a generator close to the array. It is possible that during the first few weeks of the experiment the current field was such that energy from weaker or more removed sources was carried into the experimental area causing the lower observed coherences and amplitudes. The sudden change in the direction of the current during late August and the immediate increase in tidal amplitude may indicate that the signal during segment 4 was predominately from a single, relatively close source. This explanation is consistent with the high vertical coherences observed at all moorings during segment 4, and with the high horizontal coherence between moorings B1 and B2 at the same time. It does not explain why coherences at the largest separations (B1-B4 and B2-B4) were not as high as expected.

The direction of propagation of the internal tide can be determined by assuming that the tidal signal is a plane wave or a sum of coherent modes from a single source. Although many topographic features potentially contribute to the total internal tide field in the JASIN area, the signal received by the mooring array during segment 4 appears to

be predominantly from one source. Because of the large amplitude of the signal at this time, it also may be approximated as a line spectrum. For these reasons the directional analysis of the next section concentrates on the propagation characteristics of the internal tide during segment 4.

6. Propagation Characteristics of the Semidiurnal Internal Tide

Davis and Regier (1977) discuss five different methods of estimating directional spectra from an array of sensors and compare results obtained by each when the true spectrum of the input is known. The method used here, called the beam forming method, is the most elementary of these and is also the simplest to implement. Since the maximum resolution of this method is determined by the array configuration, the resolution is generally poor for waves that have wavelengths very much longer than the largest sensor separation. However, Davis and Regier show that when the wavelengths are on the order of the largest sensor separation, the performance of the beam forming method is no worse than the more sophisticated methods.

The applicability of the beam forming method to the scales encountered in this study is demonstrated by examination of Fig. 8. A time series of two hour moving averages of isotherm depth at about 50 m calculated once an hour during segment 4 is shown for all three moorings. The internal tide at mooring B4 is consistently out of phase with observations at mooring B1, and the phase difference between observations at moorings B1 and B2 is always very small. The actual phase differences calculated from the cross-spectra between isotherms from each mooring at approximately 50 m depth are shown in Table 2. These phase differences suggest that the internal tide during segment 4 was traveling in a direction that was closer to north-south than east-west, with a wavelength of no more than twice the distance between moorings B1 and B4, or about 40 km. Smaller wavelengths are also consistent with these observations, but as discussed above, the higher modes are less likely to survive propagation through a

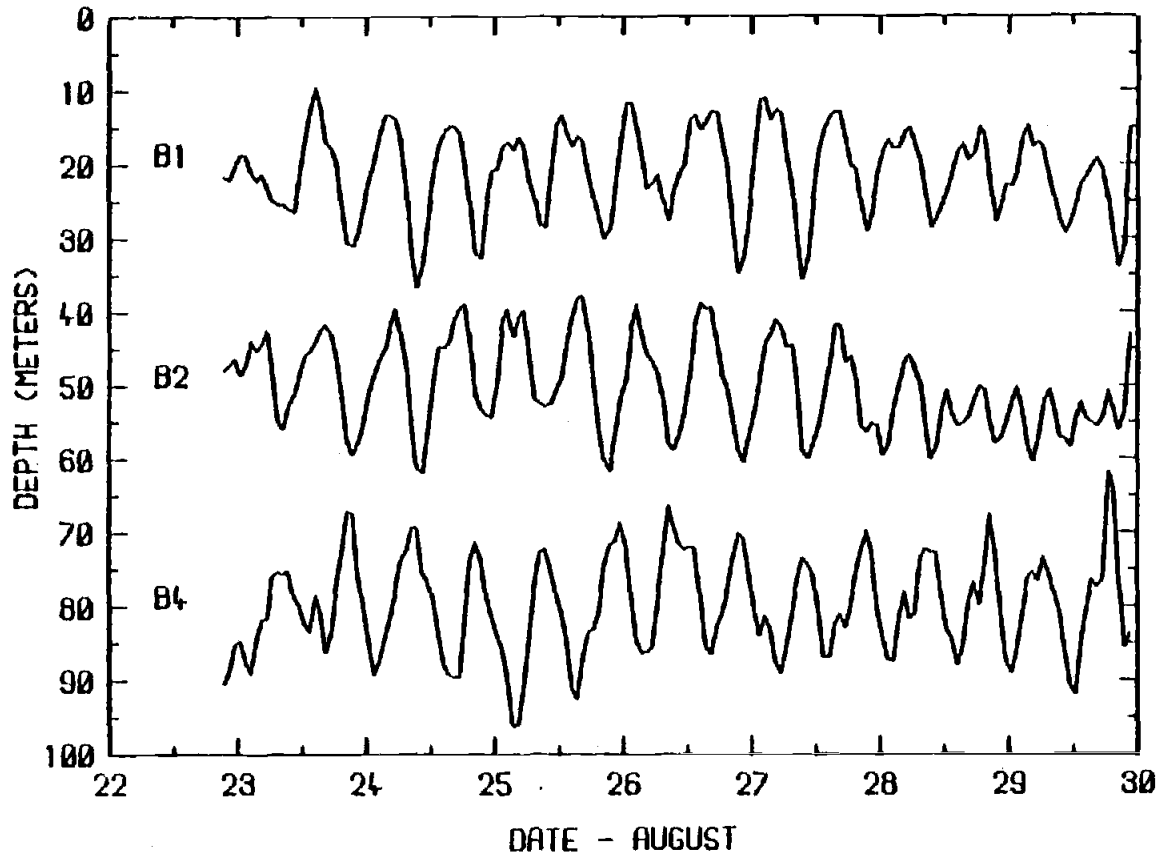

Fig. 8. Time series of two hour moving averages of isotherm depth at about 50 m calculated once every hour during segment 4. The ordinate for moorings B1 and B4 are displaced upward 30 m, and downward 30 m respectively. The isotherms are 10.8°C at B1, 10.6°C at B2, and 10.0°C at B4.

time-varying medium because of their smaller phase speeds. Waves with wavelengths more than 40 km could not produce the 180^{o} phase difference observed between moorings B1 and B4. This analysis seeks to determine the largest possible wavelength consistent with the observations of Fig. 8.

Since the wavelengths of the waves propagating through the array, about 40 km, are on the order of the largest sensor separation, about 20 km, the major limitation of the beam forming method is the configuration of the array itself. The resolution of the method is determined by the beam patterm of the array (Fig. 9a), which depends only on sensor separation. The beam pattern as a function of wavenumber $\vec{k}$ is given by

$$B(\vec{k}) = \frac{1}{M^2} \sum_{p,q=1}^{M} \exp\left[2\pi i \vec{k}\cdot(\vec{x}_p - \vec{x}_q)\right] , \qquad (2)$$

where M is the number of sensors in the array, and $\vec{x}_p$ is the location of the p^{th} sensor. An estimate of the wavenumber spectrum at frequency ω_o is

$$S(\vec{k},\omega_o) = \frac{1}{M^2} \sum_{p,q=1}^{M} \frac{f_{pq}(\omega_o) \exp\left[2\pi i \vec{k}\cdot(\vec{x}_p - \vec{x}_q)\right]}{\left[f_{pp}(\omega_o)\, f_{qq}(\omega_o)\right]^{\frac{1}{2}}} , \qquad (3)$$

where f_{pq} is the cross spectrum at frequency ω_o between observations at sensors p and q. The relationship between the beam pattern, or wavenumber window, and the two-dimensional wavenumber spectrum can be understood by considering the analagous frequency window in conventional time series analysis. The effect of finite record length can be thought of as a multiplication of the time series by a boxcar function, resulting in the convolution in frequency space of the true spectral density function with the transform of the boxcar function, sometimes called the sinc function. The net effect of this convolution when

Table 2. Phase differences observed at semidiurnal frequency at about 50 m depth during segment 4.

Mooring Pair	Separation (km)	Phase Difference (deg)
B1 - B2	5.8	-25
B1 - B4	19.2	-166
B2 - B4	19.7	-141

computing an estimate of the spectral density function at some frequency, ω_o, is to move the main peak of the sinc function to ω_o then to multiply the true spectral density function by the translated sinc function, and finally to integrate over all frequencies. Similarly, Capon (1969) shows that estimates of the wavenumber spectrum at frequency ω_o and wavenumber $\vec{k}_o$ (3) involve multiplying the beam pattern centered at $\vec{k}_o$ by the true wavenumber spectrum and integrating over all x- and y-wavenumbers.

Therefore, if a plane wave with frequency ω_o and wavenumber $\vec{k}_o$ propagates through an array, the wavenumber spectrum at ω_o will be the beam pattern reproduced with its center at $\vec{k}_o$, and an estimate of the direction and wavelength of the signal can be no better than the resolution of the beam pattern. This illustrates the importance of array design to studies of wave propagation. Davis and Regier (1977) discuss optimum array design and show that the crucial feature is the set of separations of the sensors in lag space, called the coarray. Larger separations provide for a sharper wavenumber window around the central peak in the same manner that long record lengths produce better resolution of a frequency spectrum. This is illustrated by the beam pattern of the array used in the present study (Fig. 9a). The peak at the center is much broader in the x-direction, where the largest sensor separation is 6 km, than it is in the y-direction, where the separation is almost 20 km. On the other hand, the minimum separation of the coarray affects the minimum wavenumber difference at which the beam pattern will have a secondary peak resulting in aliasing. In other words, the array cannot determine how many wavelengths lie between its most closely spaced sensors. The aliases in Fig. 9a occur every 1/20 km^{-1} in the y-direction but only every

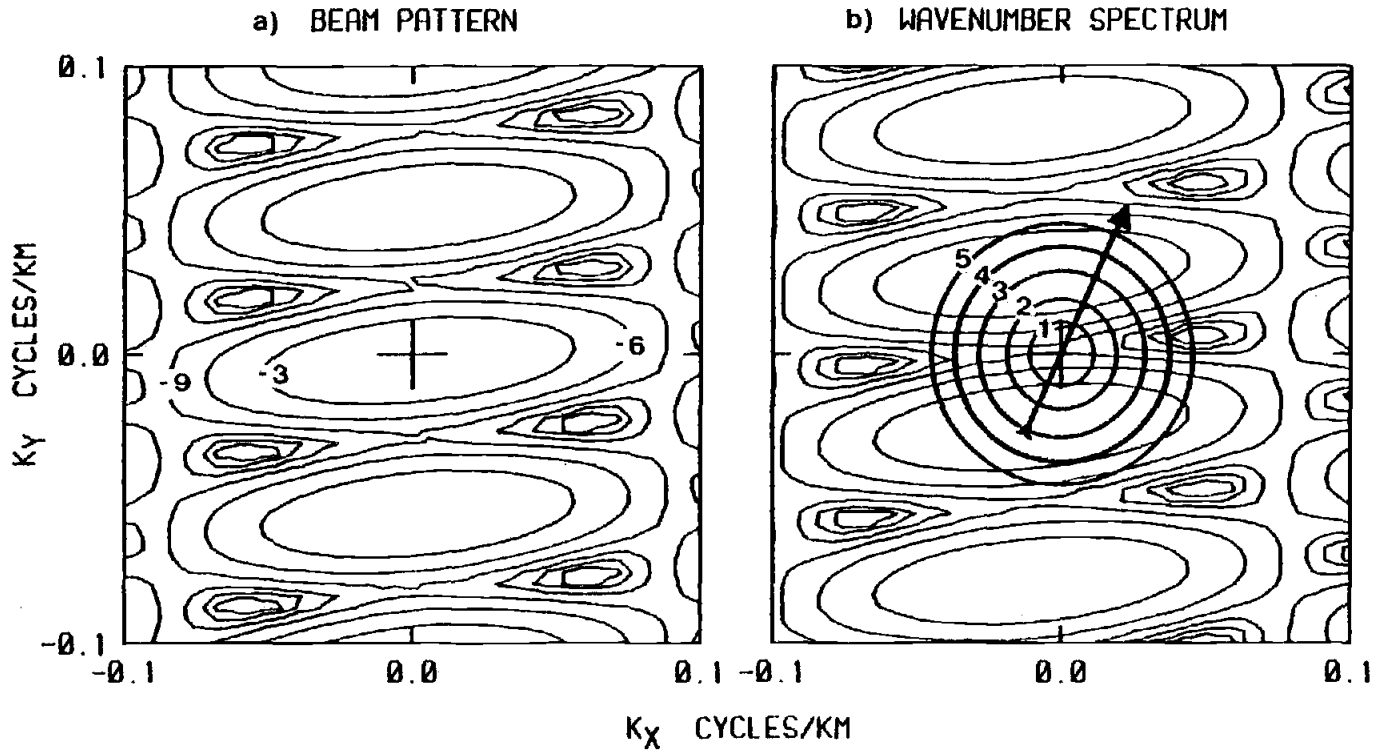

Fig. 9. Beam pattern (a) and wavenumber spectrum (b) at tidal frequency during segment 4. The peaks in these figures are the large ovals and the troughs are smaller teardrop shaped regions. Contour intervals are 3 db down from the peaks. Circles in (b) represent wavenumbers of the first five internal wave modes, and the arrow is the direction of propagation indicated by the peak in the lower left-hand quadrant.

$1/6\ km^{-1}$ in the x-direction. The ideal array for use as an antenna is then one with many sensors and few redundant lags (which provide no new information) or one with fewer sensors that has been designed as a compromise between high resolution of peaks and large spacing of aliases. The array used in this study was not designed for the measurement of directional spectra, and the broad peaks in the beam pattern show it is not an ideal antenna, but nevertheless it performs satisfactorily enough for the purpose of this analysis.

The calculated wavenumber spectrum at tidal frequency for segment 4 is shown in Fig 9b. Before discussing the interpretation of the spectrum, a few comments must be made about the method used for the calculation. Following Hendry (1977), the Fourier transform at tidal frequency has been used in computing the cross-spectrum in (3) rather than the cross-spectra formed by averaging over the tidal band. This assumes that the internal tide is best modeled as a deterministic plane wave when it arrives at the array rather than as a random process. As discussed earlier, this assumption may be reasonable for the high amplitude internal tide observations during late August (segment 4). If the signal is close to being a single plane wave, the wavenumber spectrum is always very nearly the beam pattern reproduced at the wavenumber of the signal.

Peaks in the wavenumber spectrum can then be interpreted as the most probable wavenumbers at which a plane wave is propagating through the array. A peak at wavenumber (k_x, k_y) represents a wave of wavelength $\left[1/(k_x^2 + k_y^2)^{\frac{1}{2}}\right]$ traveling in a direction defined by a vector drawn from the peak toward the origin. For example, the peak closest to the origin in the southwest quadrant of Fig. 9b is interpreted as a wave with a wavelength of about 36 km traveling toward the northwest in the direction of

the arrow shown, about 25° to the east of north. The uncertainty in this estimate is defined by the broadness of the peak in the beam pattern. The peak in the northeast quadrant that is closest to the origin also represents a wave with a wavelength of 36 km, but traveling toward the southeast, about 155° to the east of north. All peaks farther from the origin than these two represent waves with shorter wavelengths. As discussed earlier, shorter waves are less likely to survive propagation from the generator and should be interpreted as aliases of the main peak. One of the peaks closest to the origin must also be interpreted as an alias, but the coincidence that the wavelength of the internal tide is so close to twice the array dimension makes this interpretation difficult. If the wavelength were different, observations at moorings B1 and B4 would not be out of phase and both peaks would not lie the same distance from the origin.

The topography in the JASIN area provides evidence that Rockall Bank, to the southwest of the array (Fig. 1) is the most probable internal tide generator, meaning the peak in the northwest quadrant of Fig. 9b should be chosen as the alias. If the arrow drawn from the peak in the southwest quadrant of the wavenumber spectrum is superimposed on the topography in Fig. 1, it points directly from Rockall Bank toward the mooring array. Weigand et al, (1969) showed that internal waves propagate normal to bathymetric contours regardless of the angle of incidence of the barotropic wave. Generation at Rockall Bank is consistent with this. An arrow drawn in the direction indicated by the peak in the northwest quadrant of the wavenumber spectrum does not lead directly from any of the topographic features.

The topographic features can also be examined to determine their effectiveness as internal tide generators.

As discussed by Torgrimson and Hickey (1979), the internal tidal energy generated by interaction of the barotropic tide at frequency ω with a continental shelf propagates along characteristics whose slope is given by

$$\frac{dz}{dx} = \pm \left(\frac{\omega^2 - f^2}{N^2 - \omega^2} \right)^{\frac{1}{2}} , \qquad (4)$$

where f is the Coriolis parameter and N is the Brunt-Vaisala frequency. The most effective generator is one whose slope is equal to or greater than the slope of the characteristic. Profiles of topography surrounding the JASIN region are shown in Fig. 10, and the corresponding section lines are drawn in Fig. 1. Also shown is the tidal characteristic calculated by vertical integration of (4) using the JASIN mean buoyancy frequency (Fig. 4). The slope of Rockall Bank (profile A) is approximately equal to or steeper than the slope of the characteristic over the depth range from about 400 m to about 1400 m, indicating that it may be a very effective generator. Lousy Bank to the north of the array (profile C) has one of the less steep slopes in the area and may not be a good generator. The topographic feature closest to the mooring array is George Bligh Bank directly to the west (profile B). Although its slope suggests it may be an effective generator, the wavenumber spectrum indicates a very low probability that the tidal signal received at the array was generated at George Bligh Bank. It is not clear whether this is due to the character of the bank or effects of the mean current. The slopes of the remaining four profiles in Fig. 10 all suggest that these features have some degree of effectiveness as internal tide generators, but the wavenumber spectrum indicates that the internal tide was probably not from an easterly direction.

The wavenumbers, wavelengths, and phase speeds of the

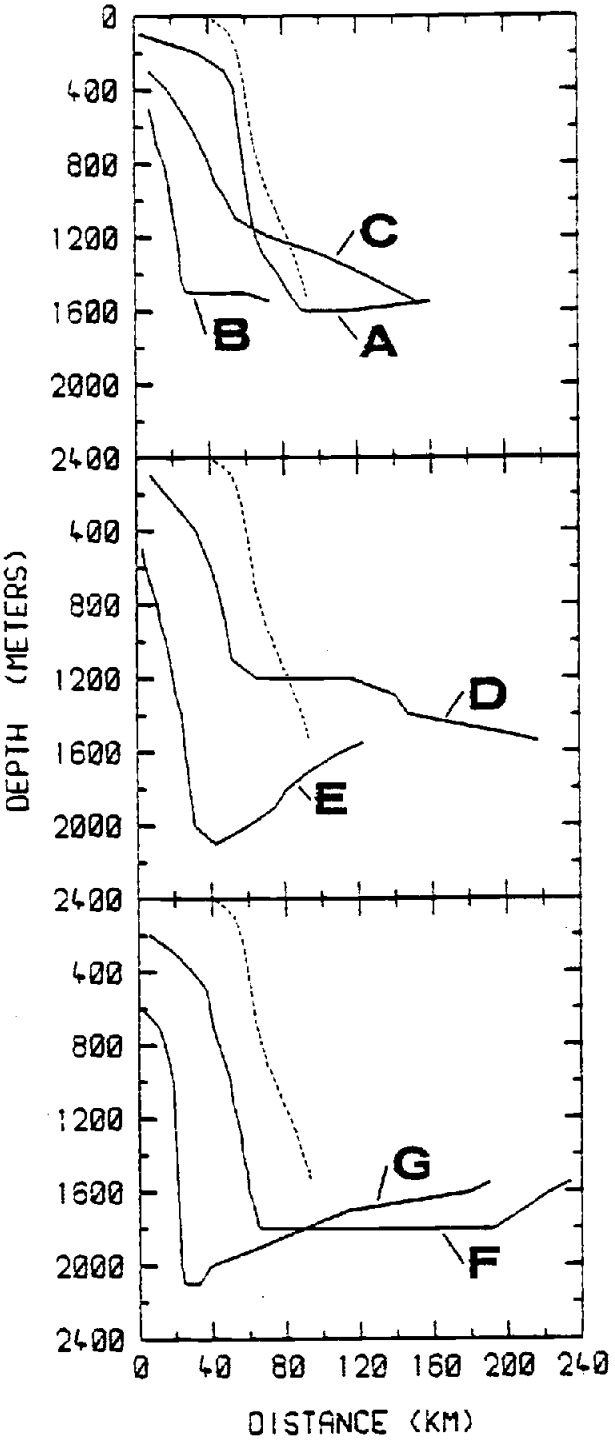

Fig. 10. Profiles of topography corresponding to section lines in Fig. 1 (solid lines), and tidal characteristic (dashed line) calculated from the mean buoyancy frequency profile.

first five modes at tidal frequency calculated from internal wave theory by M. D. Levine are given in Table 3, and circles have been drawn in Fig. 9b to represent the wavenumber of each mode. The wavelength of 36 km observed here for the internal tide suggests that mode 3 is dominant in the JASIN area. The mode 3 circle intersects the center of each of the two peaks in the wavenumber spectrum which are closest to the origin. All other aliases are much higher mode. This, however, does not rule out contributions from other modes. The wave observed here may actually be a sum of coherent modes which has not yet traveled through enough fluctuations in the mean hydrographic field to become incoherent. It is not possible to determine from this analysis whether the signal is purely mode 3 or whether it is a sum of coherent modes such that the relative contribution of each mode makes it dominantly mode 3. Fig. 9b shows there is some probability that modes 2 and 4 contribute to the structure of the internal tide, but the probability that the internal tide is dominantly mode 1 is very low.

These results are in contrast to those of Hendry (1977) who finds that the first baroclinic mode is dominant in measurements of the semidiurnal tide generated at the Blake Escarpment. Wunsch and Hendry (1972) show the second mode is dominant in measurements of the semidiurnal internal tide in the North Atlantic on the continental slope region south of Cape Cod. However, Simpson and Paulson (1979) discuss observations in the central North Pacific during POLE which suggest that most of the energy of the semidiurnal internal tide in that area is in the third order modes. They show that their results are consistent with those of Barnett and Bernstein (1975), also in the central North Pacific.

Table 3. Wavenumbers, wavelengths, and phase speeds of the first five internal wave modes at tidal frequency.

Mode	Wavenumber (km^{-1})	Wavelength (km)	Phase Speed (cm/sec)
1	1.06×10^{-2}	94.3	211.
2	1.92×10^{-2}	52.1	117.
3	2.76×10^{-2}	36.2	81.2
4	3.65×10^{-2}	27.4	61.4
5	4.47×10^{-2}	22.4	50.1

5. Conclusion

The lack of agreement between the GM spectrum and the internal wave spectra measured during JASIN suggested the proximity of generation or dissipation mechanisms of internal waves. Wind forcing did not appear to be a major source of internal wave energy in this region, as indicated by the lack of correlation between the time variation of the spectral levels and the wind speed.

However, large spectral peaks at semidiurnal frequency implied that a significant amount of energy was being added to the internal wave spectrum by conversion of barotropic energy into baroclinic motion at nearby continental shelves and other sloping topography. A week-long period of coherent, high-amplitude semidiurnal oscillations began just after an abrupt change in the direction of the mean current in late August 1978. Since the barotropic tides at this time showed no evidence of unusually large amplitudes, the current change was taken as an indication that the high amplitude event was due to a change in the generator rather than to a change in the tidal signal itself. The mooring array was used as a simple antenna and the propagation characteristics of the waves were examined by forming the two-dimensional wavenumber spectrum. The internal tide in the JASIN region was found to have a wavelength of about 36 km, making it dominantly third mode. The wavenumber spectrum and the arrangement of the nearby topographic features suggested that the internal tide propagated toward the northwest during JASIN and that the generation region was Rockall Bank, about 100 km southwest of the mooring array.

REFERENCES

Barnett, T. P., 1976: Large scale variation of the temperature field in the North Pacific Ocean. Naval Res. Rev., March, 36-51.

Capon, J., 1969: High-resolution frequency-wavenumber spectrum analysis. Proc. IEEE, 57, 1408-1418.

Davis, R. E., and L. A. Regier, 1977: Methods for estimating directional wave spectra from multi-element arrays. J. Mar. Res., 35, 453-477.

Desaubies, Y. J. F., 1976: Analytical representation of internal wave spectra. J. Phys. Oceanogr., 6, 976-981.

deWitt, L. M., J. Bottero, W. V. Burt, C. A. Paulson, and J. Simpkins, 1980: Moored temperature observations in JASIN. Report, Reference 80-15, School of Oceanography, Oregon State University, Corvallis, Oregon 97331, 127 pp.

Frankignoul, C., 1974: A cautionary note on the spectral analysis of short internal wave records. J. Geophys. Res., 79, 3459-3462.

Garrett, C., and W. Munk, 1972: Space-time scales of internal waves. Geophys. Fluid Dyn., 2, 225-264.

Garrett, C., and W. Munk, 1975: Space-time scales of internal waves: a progress report. J. Geophys. Res., 80, 291-297.

Garrett, C., and W. Munk, 1979: Internal waves in the ocean. Ann. Rev. Fluid Mech., 11, 339-369.

Gregg, M. C., and M. G. Briscoe, 1979: Internal waves, finestructure, microstructure, and mixing in the ocean. Rev. Geophys. Space Phys., 17, 1524-1548.

Hendershott, M. C., 1981: Long waves and ocean tides. Evolution of Physical Oceanography, B. A. Warren and C. Wunsch, Eds., The Massachusetts Institute of Technology, 292-341.

Hendry, R. M., 1977: Observations of the semidiurnal internal tide in the western North Atlantic Ocean. Phil. Trans. Roy. Soc. London, A286, 1-24.

Ishida, H., 1980: Analysis of meteorological observations from an array of buoys during JASIN. Report, Reference 80-2, School of Oceanography, Oregon State University, Corvallis, Oregon 97331, 63 pp.

Joyce, T. M., R. H. Kase, and W. Zenk, 1980: Horizontal advection of temperature in the seasonal thermocline during JASIN 1978. J. Phys. Oceanogr., 10, 1686-1690.

Kase, R. H., and G. Siedler, 1979: Internal wave kinematics in the upper tropical Atlantic. Deep-Sea Res., GATE Supplement I to Vol. 26, 161-189.

Levine, M. D., and R. A. deSzeoke, 1981: High frequency internal waves in the upper ocean during MILE. (to be submitted).

Muller, P., D. J. Olbers, and J. Willebrand, 1978: The IWEX spectrum. J. Geophys. Res., 83, 479-500.

Munk, W., and N. Phillips, 1968: Coherence and band structure of inertial motion in the sea. Rev. Geophys., 6, 447-472.

Pinkel, R., 1975: Upper ocean internal wave observations from FLIP. J. Geophys. Res., 80, 3892-3910.

Pollard, R. T., 1978: The Joint Air-Sea Interaction Experiment - JASIN 1978. Bull. Amer. Meteor. Soc., 59, 1310-1318.

Pollard, R. T., 1981: Inverse methods applied to the JASIN hydrographic data. JASIN News, No. 23 (unpublished manuscript).

Rattray, M., Jr., J. Dworski, and P. Kovala, 1969: Generation of long internal waves at the continental slope. Deep-Sea Res., 16, 179-195.

Regier, L. A., and R. E. Davis, 1977: Observations of the power and directional spectrum of oceanic surface waves. J. Mar. Res., 35, 433-452.

Roth, M. W., M. G. Briscoe, and C. H. McComas, III, 1981: Internal waves in the upper ocean. Accepted for publication in J. Phys. Oceanogr.

Royal Society, 1977: Air-Sea Interaction Project, Scientific Plans for 1977 and 1978. London, 208 pp.

Royal Society, 1978: Air-Sea Interaction Project, Operational Plans for 1978. London, 225 pp.

Ruddick, B. R., and T. M. Joyce, 1978: Observations of interaction between the internal wavefield and low-frequency flows in the North Atlantic. J. Phys. Oceanogr., 9, 498-517.

Simpsom, J. J., and C. A. Paulson, 1979: Observations of upper ocean temperature and salinity structure during the POLE experiment. J. Phys. Oceanogr., 9, 869-884.

Tarbell, S., M. G. Briscoe, and R. A. Weller, 1979: A compilation of moored current meter and wind recorder data volume XVIII (JASIN 1978, moorings 651-653). Woods Hole Oceanographic Institution, Woods Hole, Mass. 02543, Technical Report W.H.O.I.-79-64, 201 pp.

Thorpe, S. A., 1975: The excitation, dissipation and interaction of internal waves in the deep ocean. J. Geophys. Res., 80,328-338.

Torgrimson, G. M., and B. M. Hickey, 1979: Barotropic and baroclinic tides over the continental slope and shelf off Oregon. J. Phys. Oceanogr., 27, 241-259.

Weigand, J. G., H. Farmer, S. Prinsenberg and M. Rattray, Jr., 1969: Effects of friction and surface tide angle of incidence on the coastal generation of internal tides. J. Mar. Res., 27, 241-259.

Wunsch, C., 1975a: Internal tides in the ocean. Rev. Geophys. Space Phys., 13, 167-182.

Wunsch, C., 1975b: Deep ocean internal waves: what do we really know? J. Geophys. Res., 80, 339-343.

Wunsch, D., 1976: Geographical variability of the internal wave field: a search for sources and sinks. J. Phys. Oceanogr., 6, 471-485.

Wunsch, C., and R. Hendry, 1972: Array measurements of the bottom boundary layer and the internal wave field on the continental slope. Geophys. Fluid Dyn., 4, 101-145

Wunsch, C., and S. Webb, 1979: The climatology of deep ocean internal waves. J. Phys. Oceanogr., 9, 235-243.

van Aken, H., and G. Prangsma, 1981: Fronts and meanders in the LSA. JASIN News, No. 23 (unpublished manuscript).

APPENDIX

APPENDIX

Representative Scectra from Moorings B1, B2, and B4

The following table lists the isotherms for which spectra are presented. In general, isotherms were chosen to represent the depth range of the temperature sensors during a given segment. The isotherm for each segment of each mooring whose mean depth was closest to 50 m was used in Figs. 6 and 7 as indicated by (*) next to the mean depth. The spectra were calculated as described in the text except that band averaging was performed in 10 non-overlapping frequency bands per decade over the entire frequency range. The time periods corresponding to the 1024 point segments used for spectral analysis are given in Table 1.

Mooring	Segment	Isotherm (°C)	Mean Depth (m)	Page
B1	1	12.4	23.03	50
		12.2	25.02	50
		10.6*	47.17	50
		10.4	57.07	50
	2	12.4	25.05	51
		12.2	26.58	51
		10.6*	50.00	51
		10.4	56.31	51
	3	10.8	46.75	52
		10.6*	50.68	52
		10.4	55.34	52
		10.2	61.42	52
	4	11.2	48.44	53
		11.0*	49.77	53
		10.2	56.24	53
		10.0	59.44	53
	5	10.8	47.29	54
		10.6*	49.28	54
		10.2	54.42	54
		10.0	58.30	54
B2	1	12.0	24.80	55
		11.8	26.37	55
		10.4	44.85	55
		10.2*	52.53	55
		10.0	59.99	56
		9.8	66.87	56
	2	12.4	25.85	56
		12.2	27.28	56
		10.4*	50.90	57
		10.2	57.54	57
		10.0	64.39	57
	3	10.8	45.78	58
		10.6*	48.77	58
		10.2	57.29	58
		10.0	63.01	58
	4	10.6*	50.10	59
		10.4	51.53	59
		9.8	59.43	59
		9.6	64.65	59
	5	10.4*	49.44	60
		10.2	51.81	60
		9.8	58.48	60
		9.6	63.83	60

Mooring	Segment	Isotherm (°C)	Mean Depth (m)	Page
B4	1	11.8	24.29	61
		11.6	26.21	61
		10.2*	47.60	61
		10.0	53.65	61
		9.8	60.00	62
	2	11.8	23.37	62
		11.6	25.20	62
		10.0*	50.61	63
		9.8	56.53	63
		9.6	63.48	63
	3	10.2	44.58	64
		10.0*	48.81	64
		9.6	53.55	64
		9.4	59.53	64
	4	10.0*	49.93	65
		9.8	52.91	65
		9.6	57.53	65
		9.4	64.59	65

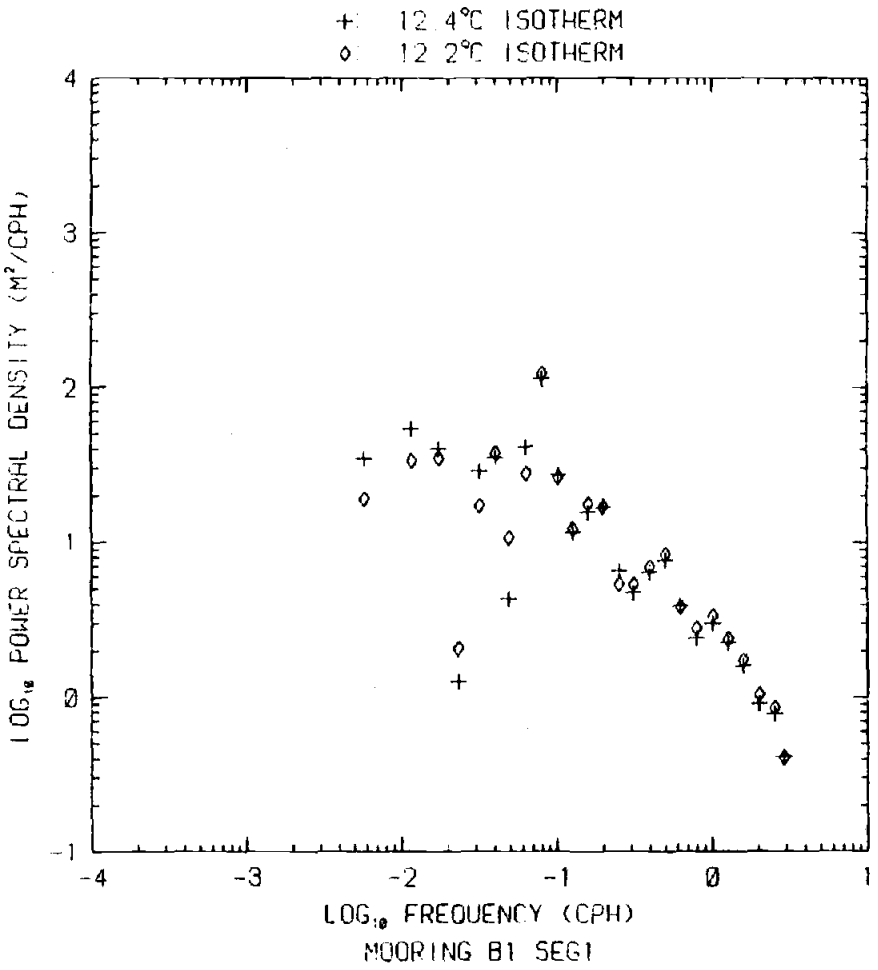
+ 12.4°C ISOTHERM
◊ 12.2°C ISOTHERM
LOG10 POWER SPECTRAL DENSITY (M²/CPH)
LOG10 FREQUENCY (CPH)
MOORING B1 SEG1

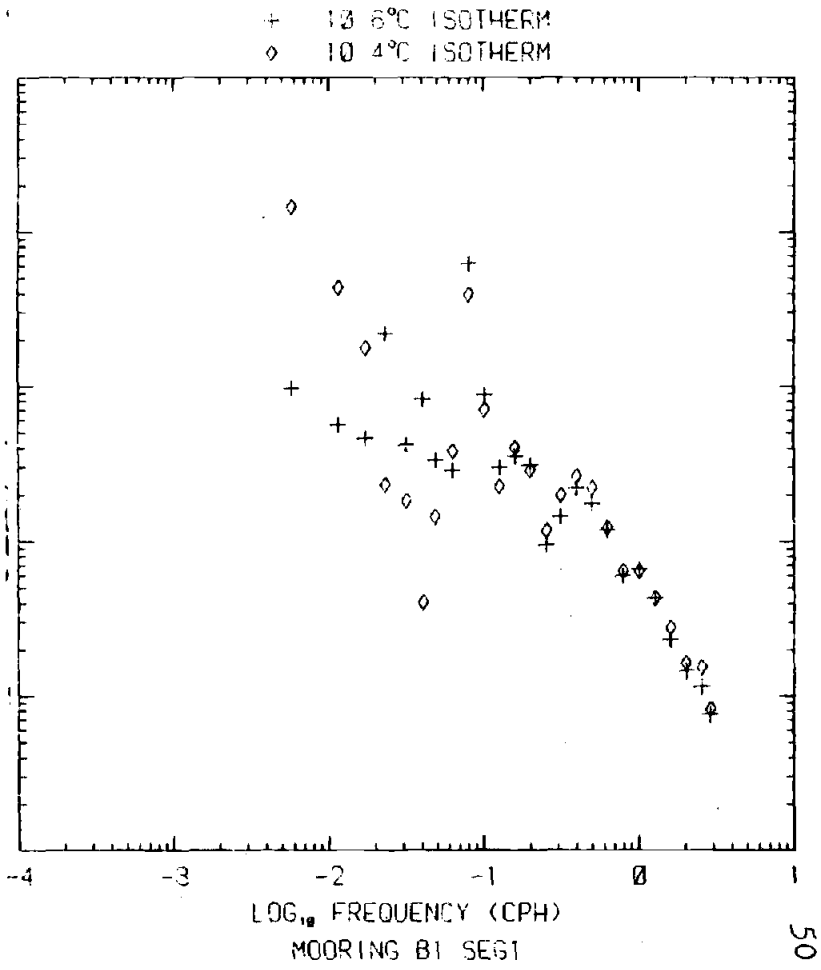
+ 10.6°C ISOTHERM
◊ 10.4°C ISOTHERM
LOG10 FREQUENCY (CPH)
MOORING B1 SEG1

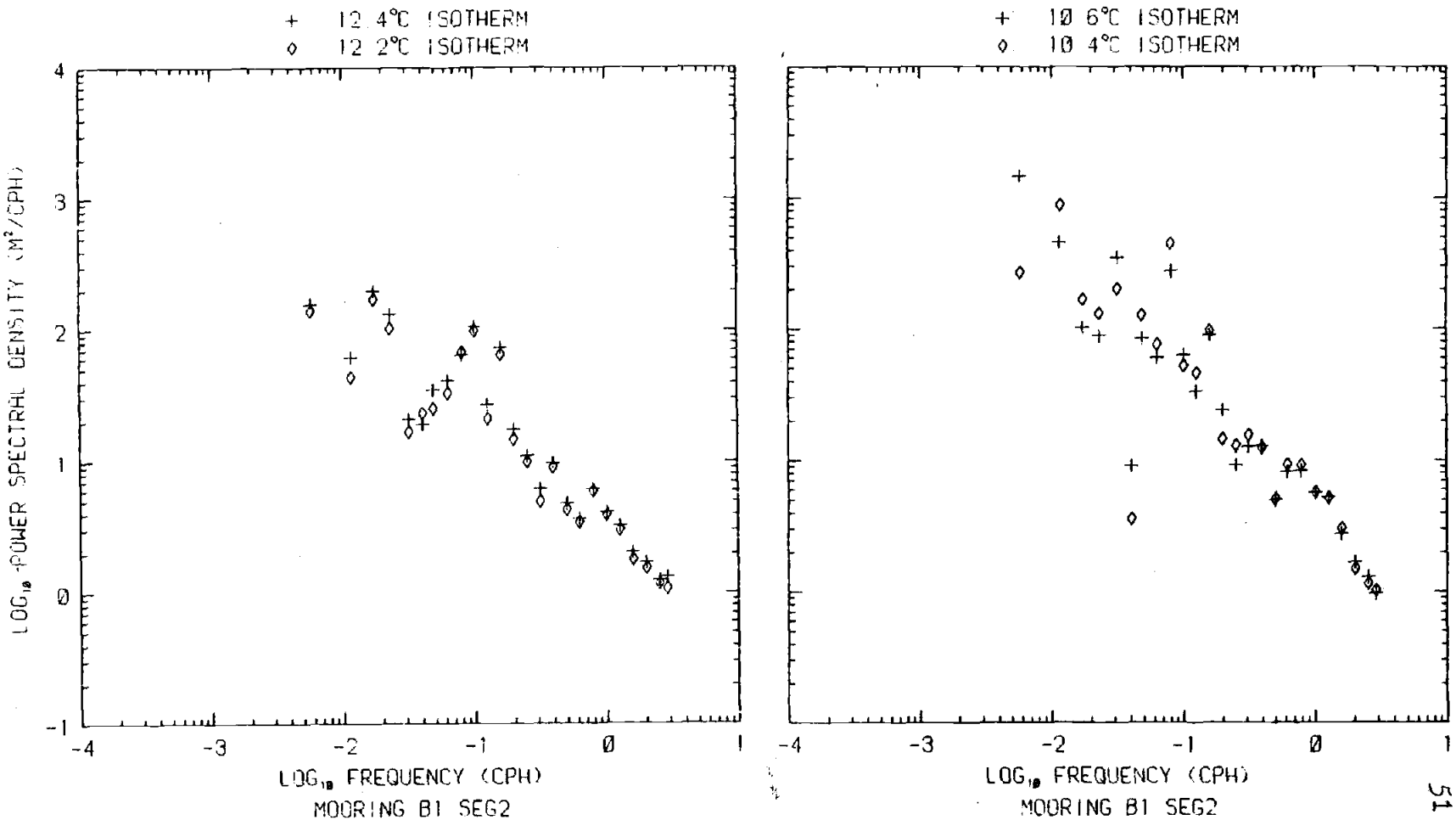
+ 12.4°C ISOTHERM
◊ 12.2°C ISOTHERM
LOG10 POWER SPECTRAL DENSITY (M²/CPH)
LOG10 FREQUENCY (CPH)
MOORING B1 SEG2
+ 10.6°C ISOTHERM
◊ 10.4°C ISOTHERM
LOG10 FREQUENCY (CPH)
MOORING B1 SEG2

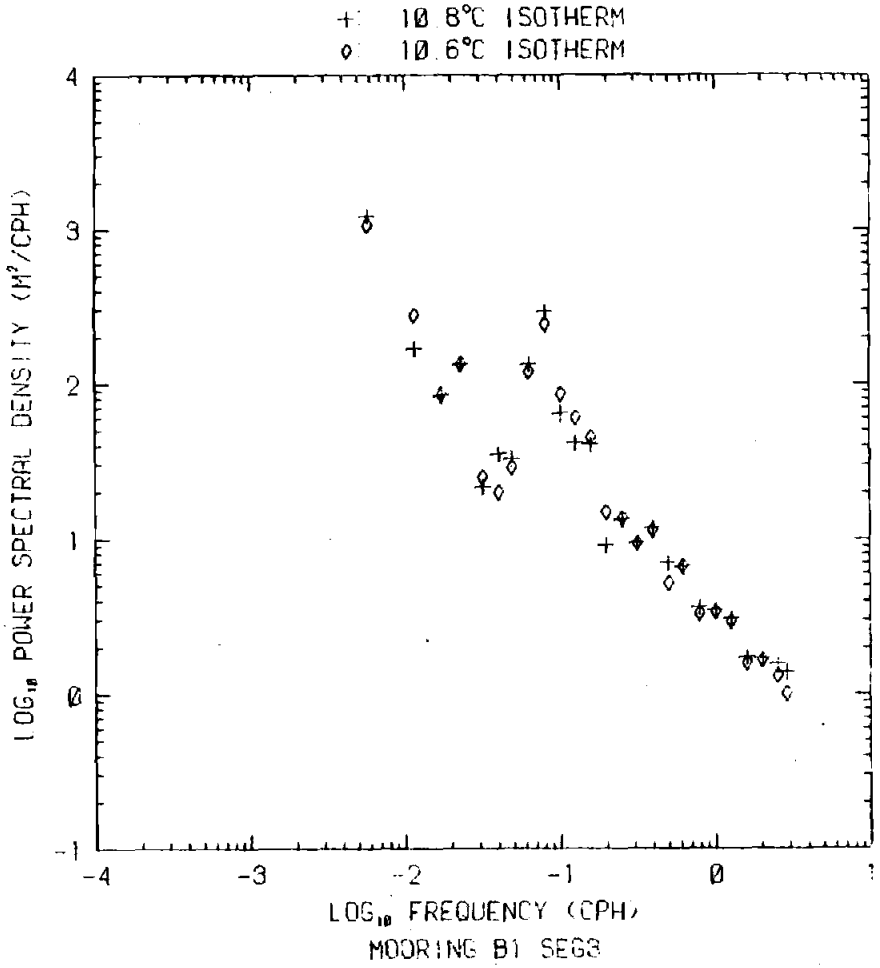
+ 10.8°C ISOTHERM
◊ 10.6°C ISOTHERM
LOG10 POWER SPECTRAL DENSITY (M²/CPH)
4
3
2
1
0
-1
-4
-3
-2
-1
0
1
LOG10 FREQUENCY (CPH)
MOORING B1 SEG3

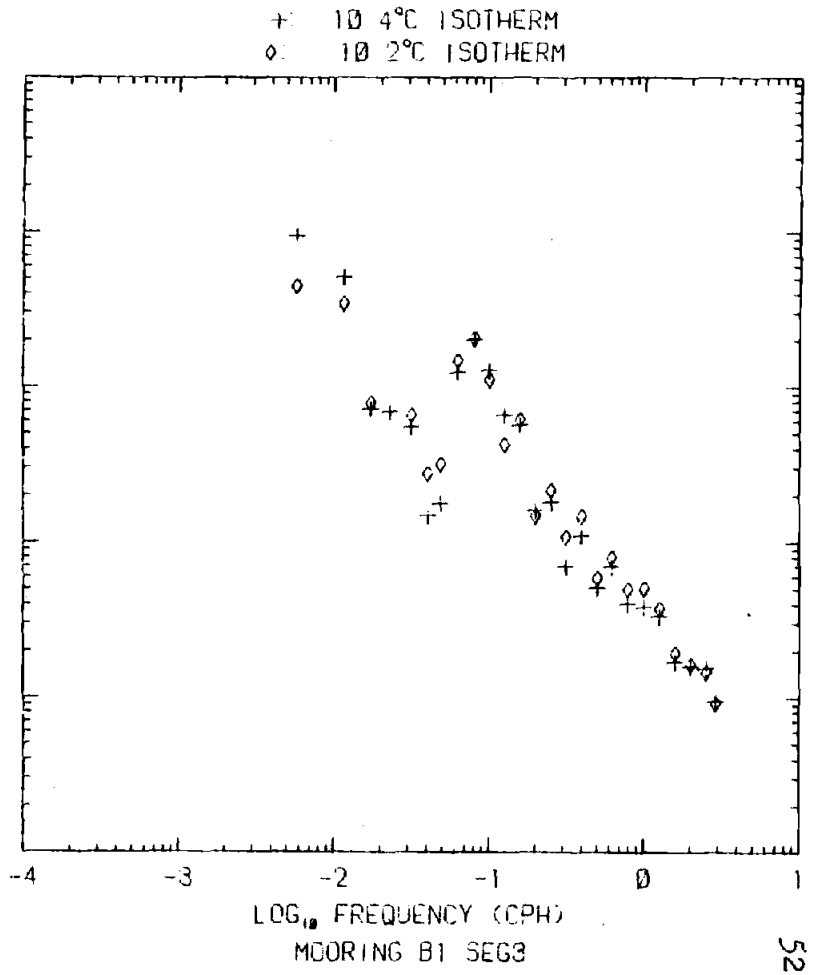
+ 10.4°C ISOTHERM
◊ 10.2°C ISOTHERM
-4
-3
-2
-1
0
1
LOG10 FREQUENCY (CPH)
MOORING B1 SEG3

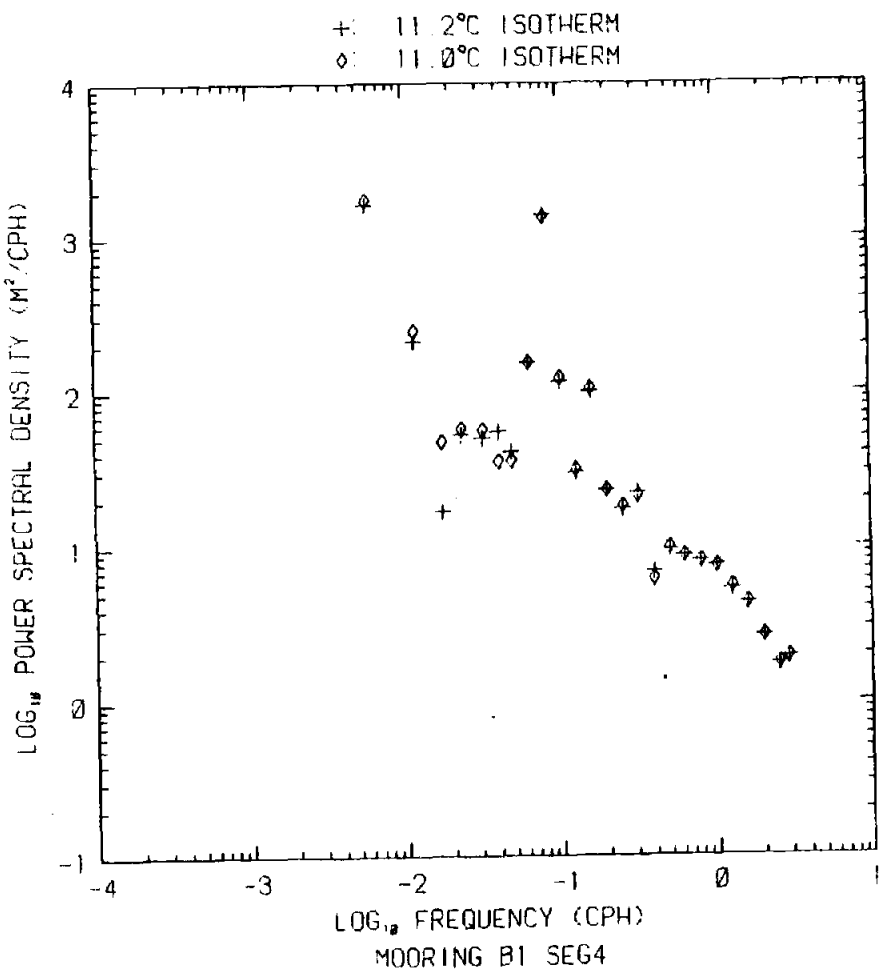
+: 11.2°C ISOTHERM
◇: 11.0°C ISOTHERM
LOG10 POWER SPECTRAL DENSITY (M²/CPH)
4
3
2
1
0
-1
-4
-3
-2
-1
0
1
LOG10 FREQUENCY (CPH)
MOORING B1 SEG4

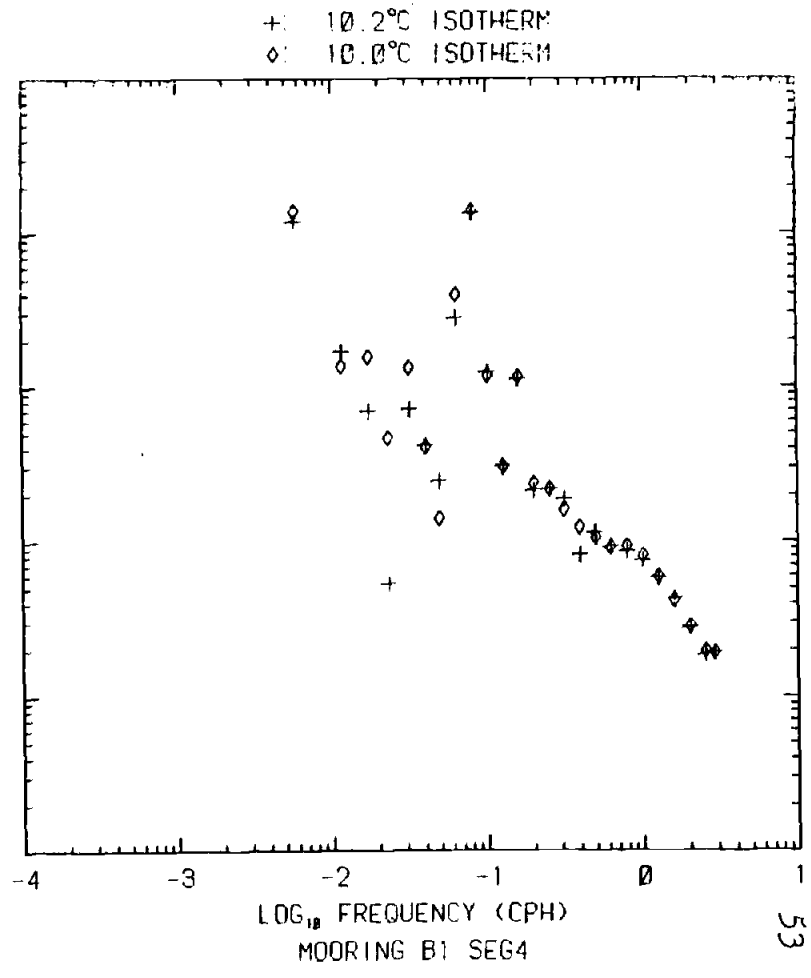
+: 10.2°C ISOTHERM
◇: 10.0°C ISOTHERM
-4
-3
-2
-1
0
1
LOG10 FREQUENCY (CPH)
MOORING B1 SEG4

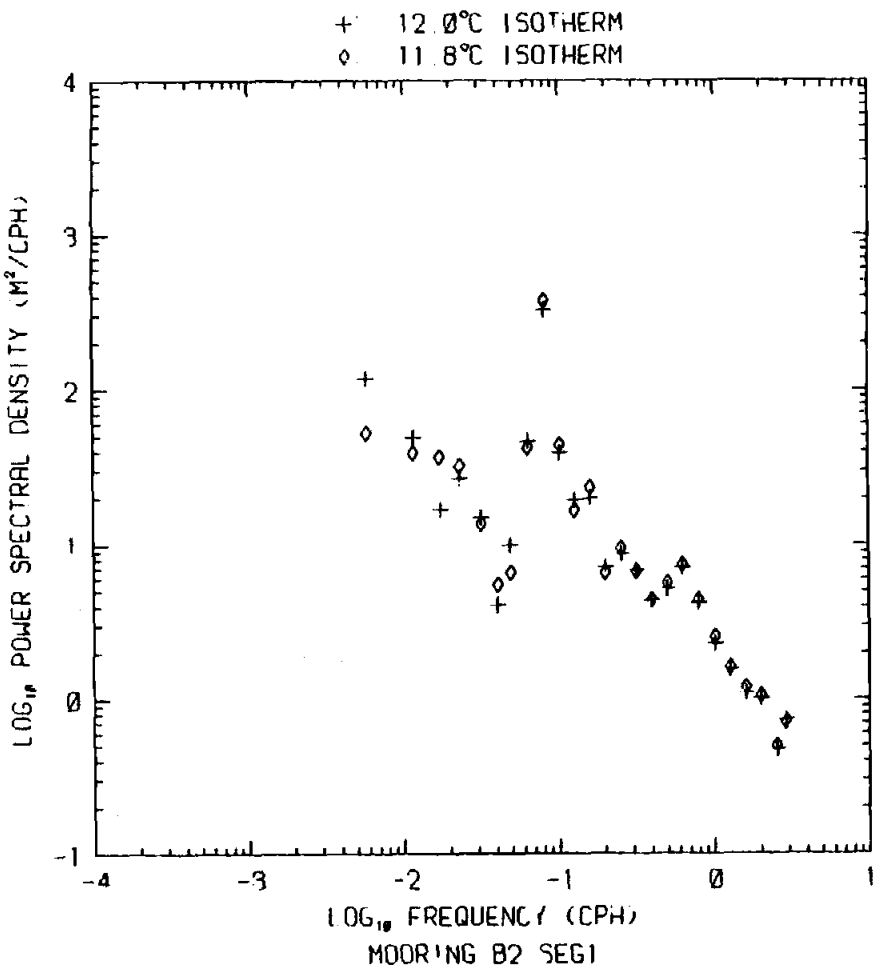
+ 12.0°C ISOTHERM
◊ 11.8°C ISOTHERM
LOG10 POWER SPECTRAL DENSITY (M²/CPH)
4
3
2
1
0
-1
-4
-3
-2
-1
0
1
LOG10 FREQUENCY (CPH)
MOORING B2 SEG1

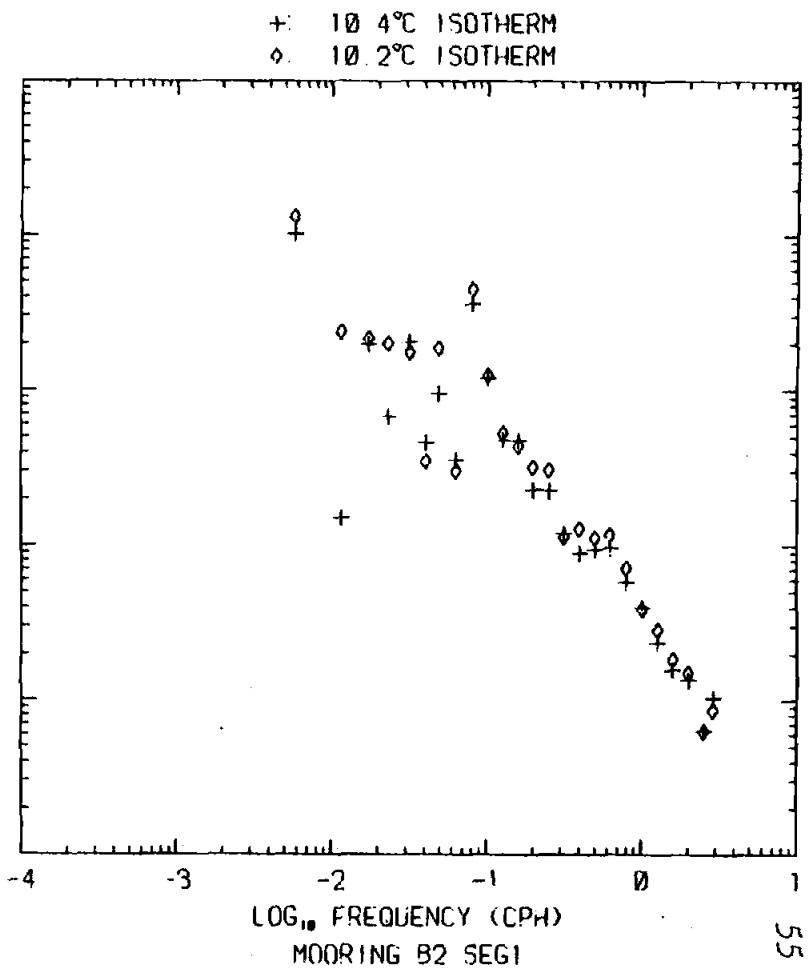
+ 10.4°C ISOTHERM
◊ 10.2°C ISOTHERM
-4
-3
-2
-1
0
1
LOG10 FREQUENCY (CPH)
MOORING B2 SEG1

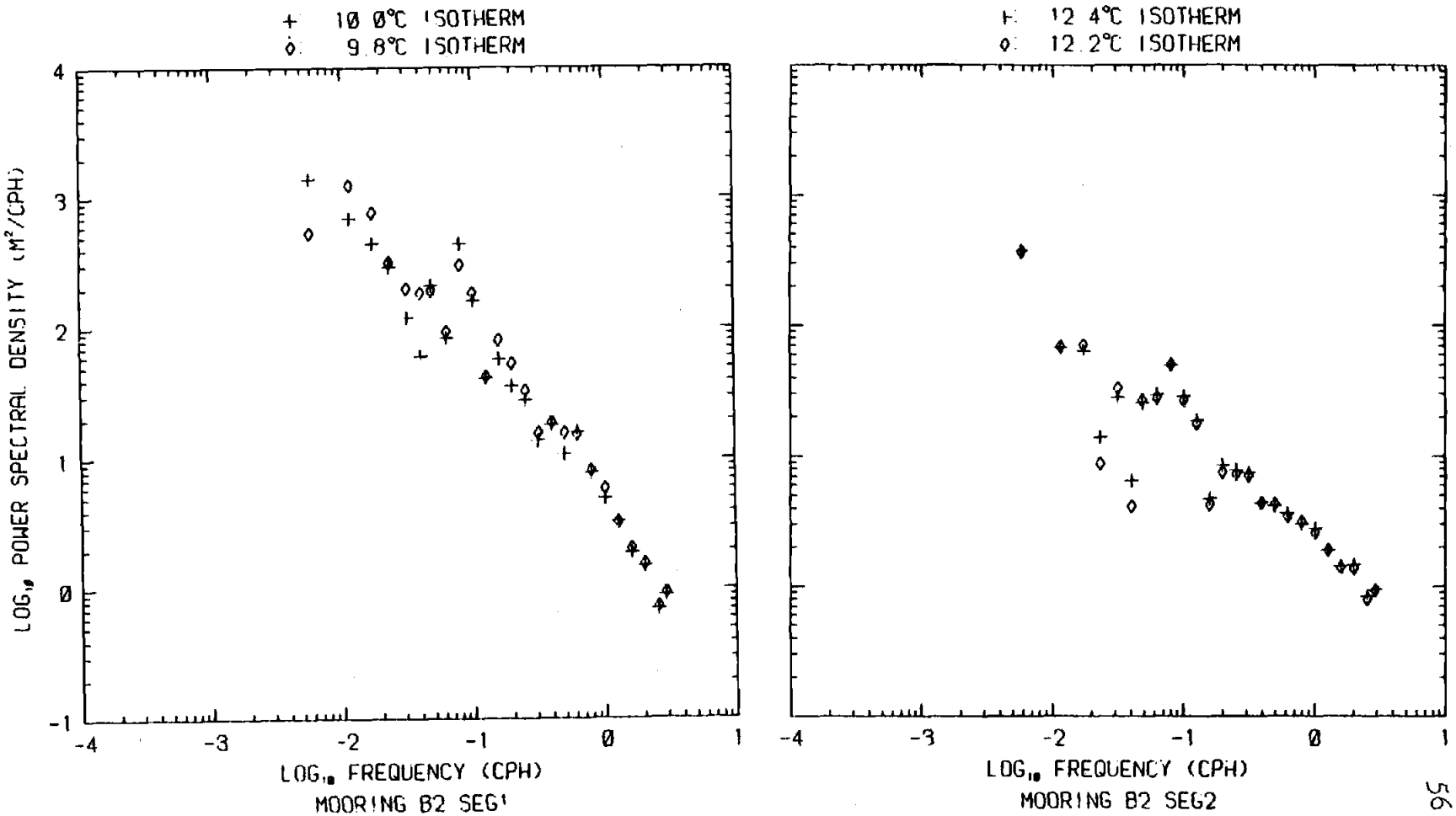
+ 10.0°C ISOTHERM
◊ 9.8°C ISOTHERM
LOG10 POWER SPECTRAL DENSITY (M²/CPH)
LOG10 FREQUENCY (CPH)
MOORING B2 SEG1
+ 12.4°C ISOTHERM
◊ 12.2°C ISOTHERM
LOG10 FREQUENCY (CPH)
MOORING B2 SEG2

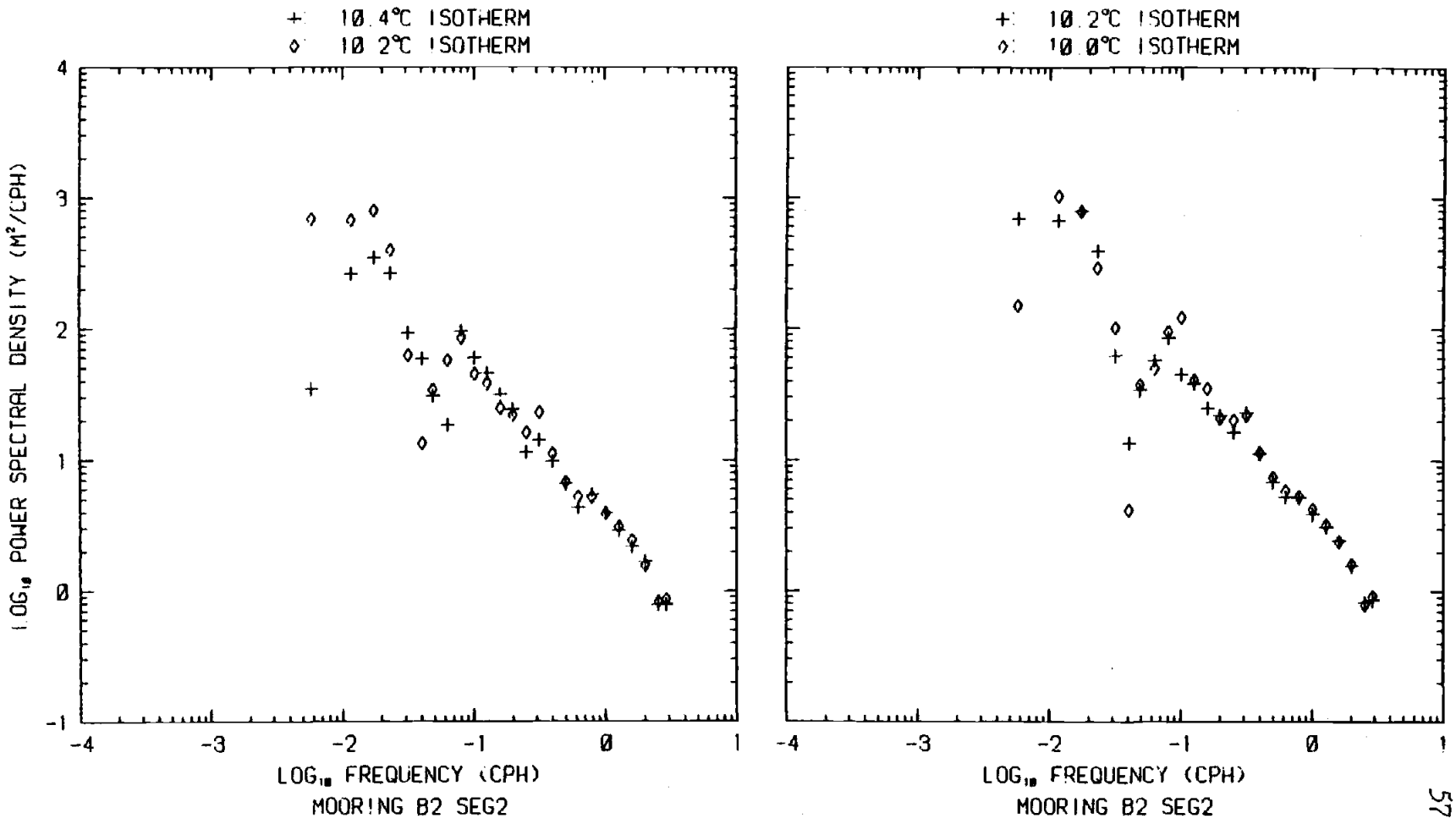
+ 10.4°C ISOTHERM
◊ 10.2°C ISOTHERM
LOG10 POWER SPECTRAL DENSITY (M²/CPH)
LOG10 FREQUENCY (CPH)
MOORING B2 SEG2
+ 10.2°C ISOTHERM
◊ 10.0°C ISOTHERM
LOG10 FREQUENCY (CPH)
MOORING B2 SEG2

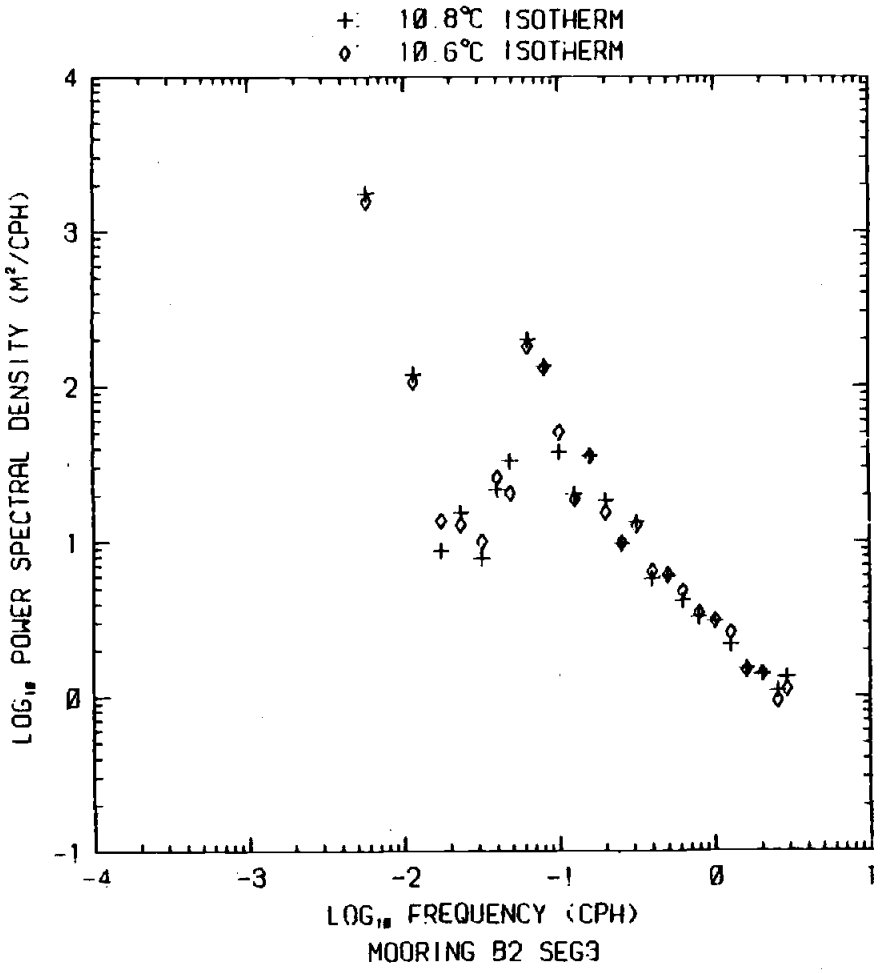
+: 10.8℃ ISOTHERM
◊: 10.6℃ ISOTHERM
LOG10 POWER SPECTRAL DENSITY (M²/CPH)
4
3
2
1
0
-1
-4
-3
-2
-1
0
1
LOG10 FREQUENCY (CPH)
MOORING B2 SEG3

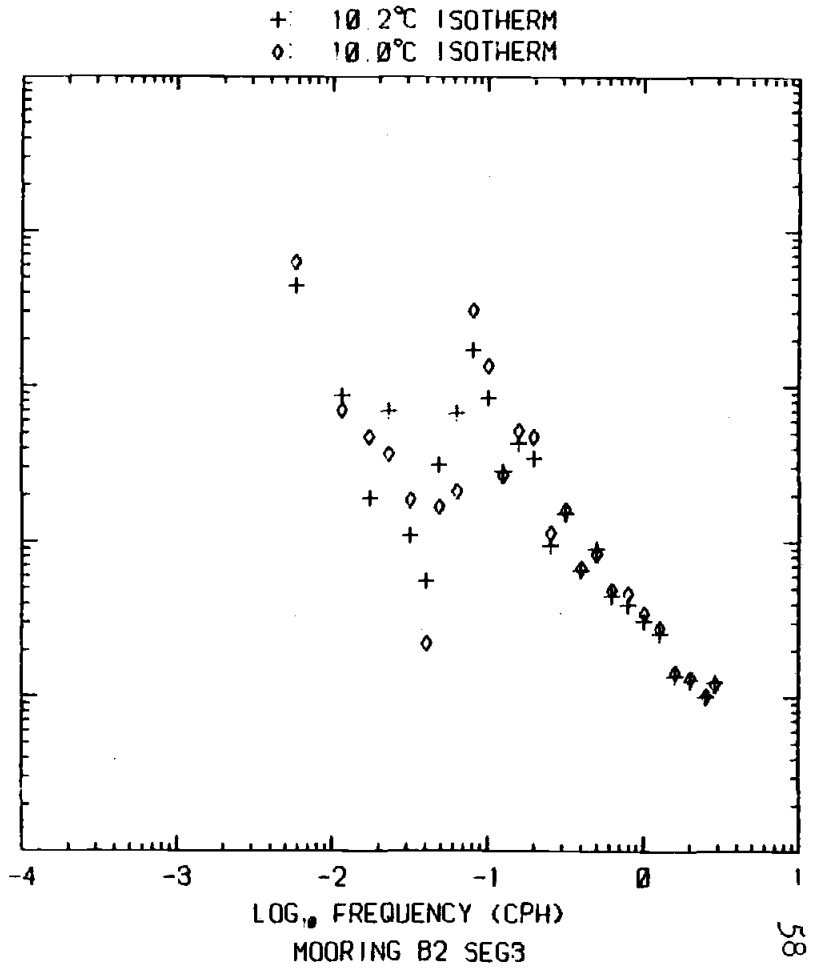
+: 10.2℃ ISOTHERM
◊: 10.0℃ ISOTHERM
-4
-3
-2
-1
0
1
LOG10 FREQUENCY (CPH)
MOORING B2 SEG3

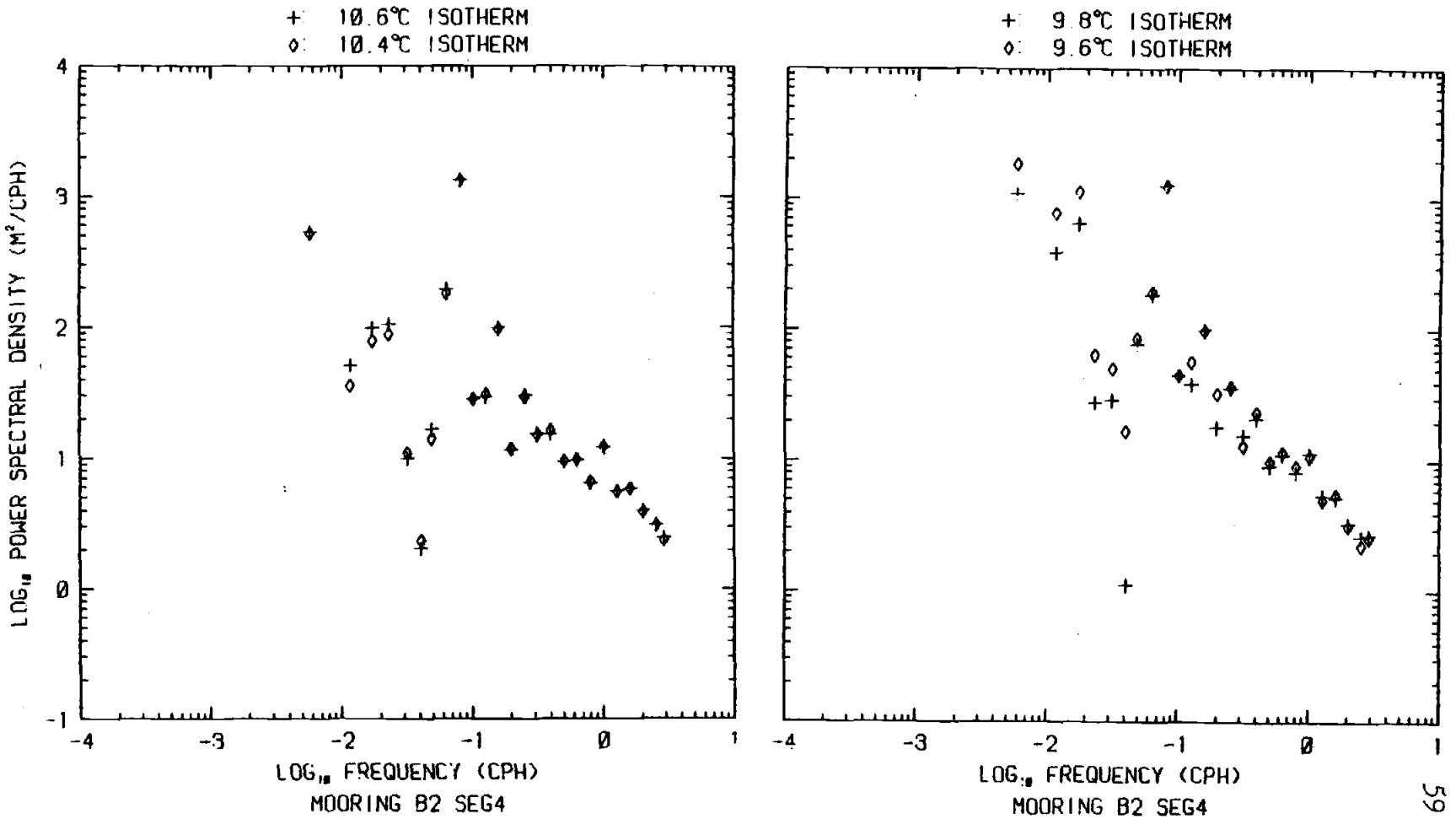
+ 10.6°C ISOTHERM
◊ 10.4°C ISOTHERM
LOG10 POWER SPECTRAL DENSITY (M²/CPH)
4
3
2
1
0
-1
-4
-3
-2
-1
0
1
LOG10 FREQUENCY (CPH)
MOORING B2 SEG4
+ 9.8°C ISOTHERM
◊ 9.6°C ISOTHERM
-4
-3
-2
-1
0
1
LOG10 FREQUENCY (CPH)
MOORING B2 SEG4

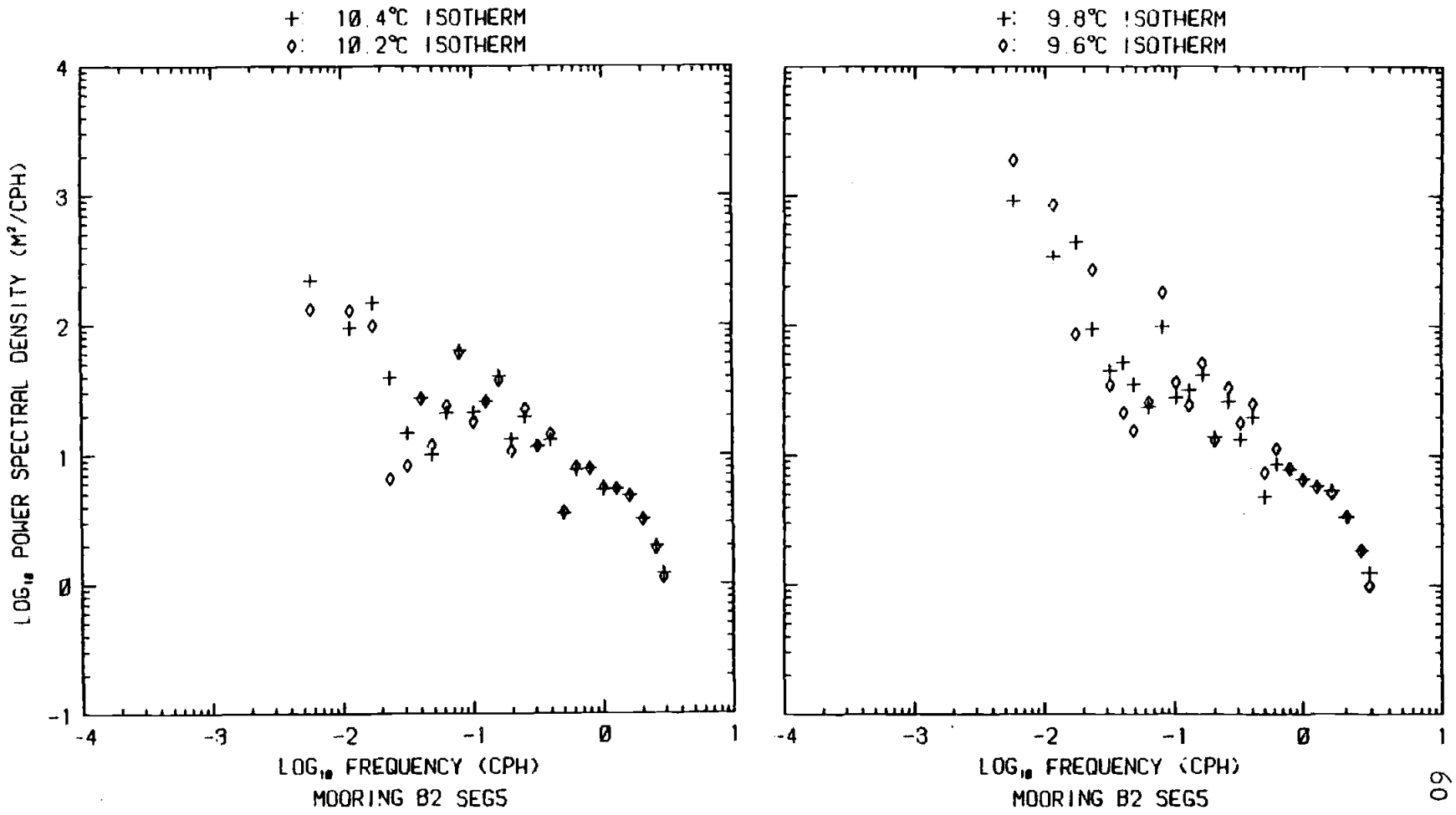
+: 10.4°C ISOTHERM
◊: 10.2°C ISOTHERM
+: 9.8°C ISOTHERM
◊: 9.6°C ISOTHERM
LOG10 POWER SPECTRAL DENSITY (M²/CPH)
LOG10 FREQUENCY (CPH)
MOORING B2 SEGS
LOG10 FREQUENCY (CPH)
MOORING B2 SEGS
4
3
2
1
0
-1
-4
-3
-2
-1
0
1